"Optimization of welding parameters to study the weld on bead of AA6082 by using Cold Metal Transfer (CMT) welding process"

A PROJECT REPORT

SUBMITTED IN THE PARTIAL FULFILMENT OF THE REQUIREMENTS
FOR THE AWARD OF DEGREE
OF

MASTER OF TECHNOLOGY
IN
PRODUCTION ENGINEERING

Submitted By

Harshit Bansal
(2K21/PRD/05)

Under the supervision of

Dr. N. Yuvraj
Assistant Professor
Department of Mechanical Engineering
Delhi Technological University, Delhi

DEPARTMENT OF MECHANICAL ENGINEERING
DELHI TECHNOLOGICAL UNIVERSITY
(Formerly Delhi College of Engineering)
Bawana Road, Delhi-110042

June, 2023

DEPARTMENT OF MECHANICAL ENGINEERING
DELHI TECHNOLOGICAL UNIVERSITY
(Formerly Delhi College of Engineering)
Bawana Road, Delhi-110042

DECLARATION

I, Harshit Bansal, 2K21/PRD/05 student of M.Tech (PRD), certify that the work which is being presented in this thesis entitled "**Optimization of welding parameters to study the weld on bead of AA6082 by using Cold Metal Transfer (CMT) welding process**" in the partial fulfilment of requirement of requirement for the award of degree of Master in Technology submitted in Department of Mechanical Engineering at Delhi Technological University, is an authentic record of my own work carried out during a period from August 2022 to May 2023, under the supervision of DR. N. YUVARAJ , Department of Mechanical Engineering, Delhi Technological University, Delhi. The matter presented in this thesis has not been submitted in any other University/Institute for the award of any degree or diploma.

Place: Delhi **Harshit Bansal**

Date: June, 2023 (**2K21/PRD/05)**

DEPARTMENT OF MECHANICAL ENGINEERING
DELHI TECHNOLOGICAL UNIVERSITY
(Formerly Delhi College of Engineering)
Bawana Road, Delhi-110042

CERTIFICATE

I hereby certify that the thesis entitled **"Optimization of welding parameters to study the weld on bead of AA6082 by using Cold Metal Transfer (CMT) welding process"** submitted to the Delhi Technological University, Delhi, is fulfilment of the requirements for the award of degree of Master of Technology in Mechanical Engineering embodies the original research work carried out by **Mr. Harshit Bansal**, Enrollment No: **2K21/PRD/05** under my supervision. This work has not been submitted in part or full for any other degree of this or any other University.

Place: Delhi

Date:

Dr. N. Yuvraj

SUPERVISOR

Assistant Professor

Department of Mechanical Engineering
Delhi Technological University
(Formerly Delhi College of Engineering)
Bawana Road, Delhi-110042

ACKNOWLEDGEMENT

I am greatly indebted to my supervisor Dr. N. Yuvraj Department of Mechanical Engineering, Delhi Technological University, Delhi, for his invaluable guidance, constant inspiration, numerous suggestions and continued support throughout this research work. I am profoundly grateful to him with reverence for helping me with necessary information and equipment & materials as well.

I would also thank with much appreciation the people whose help and support were a great asset; the technical staff at DTU, namely, Mr. Girish Anand, Mr. Lalan Kumar Sinha, who provided great help for conducting the experiments and material characterization; Mr. Tek Chand for his help in revealing the microstructures and Mr. Om Prakash for his help in microhardness testing.

Finally, I dedicate my work to my Parents. My sincere thanks to my father Mr. Jaiprakash Bansal and my mother Mrs. Rekha Devi for their support and blessings that greatly helped me carrying out this research work.

HARSHIT BANSAL

2K21/PRD/05

ABSTRACT

Aluminium alloys are extensively employed in industries such as construction, automobile manufacturing, and spacecraft production owing to their remarkable attributes, including outstanding corrosion resistance, a high strength-to-weight ratio, excellent machinability, and ductility. The cold metal transfer technique shows potential as a welding method for constructing aluminium structures. This research work focuses on a comparison of influence of activated flux on microstructure and characteristics of weld bead geometry of Al-Mg-Si alloy AA6082 manufactured by cold metal transfer (CMT) process. ER4043 was used as a filler wire to make weld on bead on 3 mm thick AA6082 plates. Various input process parameters i.e., current (80, 100 and 110 A) and welding speed (30, 40, 50 cm/min) were used, whereas the nozzle tip distance andshielding gas flow rate remained fixed at 10 mm and 15 l/min, respectively. Optical microscopyis used to study the microstructural characteristics. The samples created with activated flux have a highlevel of penetration and percentage dilution. Also, there is an increase in micro-hardness of samples which are fabricated using activated flux.

Keywords: CMT, AA6082, ER4043, weld bead geometry, activated flux, dilution, microstructure, micro-hardness, and heat input.

TABLE OF CONTENTS

LIST OF FIGURES

LIST OF TABLES

LIST OF ABBREVIATIONS

AA	Aluminium Association
Al	Aluminium
ANOVA	Analysis of variance
ASTM	American Society for Testing Materials
BM	Base Metal
CMT	Cold Metal Transfer
CTWD	Contact Tip to Workpiece Distance
DOE	Design of Experiments
DOP	Depth of Penetration
EDM	Electric Discharge Machining
FB	Flux Bead
FL	Fusion Line
FZ	Fusion Zone
GMAW	Gas Metal Arc Welding
GTAW	Gas Tungsten Arc Welding
HAZ	Heat Affected Zone
MMC	Metal Matrix Composite
RSM	Response Surface Methodology
THI	Thermal Heat Input
TIG	Tungsten Inert Gas
WFB	With Flux Bead
WFS	Wire Feed Speed
WM	Weld Zone / Weld Metal

CHAPTER 1

INTRODUCTION

1.1. INTRODUCTION

Fusion welding has been acknowledged as a crucial enabling technique to improve the innovative and sustainable production among the many manufacturing technologies [1]. Aluminum alloys are investigated to produce a cost-effective, weight-optimized body that offers excellent strength and stiffness in contemporary industrial applications including vehicle manufacture, aeroplane construction, and shipbuilding. Even though aluminium is a great material in its pure form, it could not be strong enough for applications requiring high durability. It can therefore be combined with other elements to create alloys that are significantly stronger and more appropriate for industrial usage [2]. An "alloy" is a mixture of various metallic elements that is frequently produced to increase the strength and endurance of the material. Depending on the use, pure aluminium is frequently mixed with other elements such as silicon, manganese, tin, copper, and magnesium to create aluminium alloys. With the correct combination, aluminium can probably get stronger and, in some circumstances, even surpass steel [3-5]. Alloys are less expensive while providing benefits comparable to those of pure aluminium.

1.2. APPLICATIONS OF ALUMINIUM ALLOY

Aluminium alloy is a type of metal that contains aluminium as its primary component, along with one or more additional elements, such as copper, zinc, magnesium, or silicon. This alloy has become increasingly popular due to its lightweight, corrosion-resistant, and strong properties, making it a useful material in various applications [6]. Here are some detailed applications of aluminium alloy:

1. **Transportation:** Aluminium alloy is widely used in the transportation industry due to its lightweight and strength. It is commonly used in the manufacture of aircraft, cars, trains, and bicycles. The use of aluminium alloy in transportation vehicles helps to increase fuel efficiency and reduce carbon emissions.
2. **Construction:** Aluminium alloy is used in the construction industry due to its corrosion-resistant properties and strength. It is used to make windows, doors,

roofing, and cladding. Aluminium alloys are also used in the manufacture of scaffolding, ladders, and other construction equipment.

3. **Packaging:** Aluminium alloy is used in the packaging industry because it is lightweight, durable, and can be easily formed into different shapes. It is commonly used to make beverage cans, food packaging, and cosmetic containers.
4. **Electrical and electronic equipment:** Aluminium alloy is used in the manufacture of electrical and electronic equipment due to its good conductivity, heat dissipation, and strength. It is used in the production of heat sinks, computer casings, and mobile phone casings.
5. **Sports equipment**: Aluminium alloy is used in the manufacture of sports equipment due to its lightweight and strength. It is used to make bicycle frames, baseball bats, golf clubs, and tennis rackets.
6. **Marine industry:** Aluminium alloy is used in the marine industry due to its corrosion-resistant properties. It is used to make boat hulls, masts, and fittings.
7. **Medical equipment:** Aluminium alloy is used in the medical industry due to its non-toxicity, non-magnetic, and corrosion-resistant properties. It is used to make medical instruments, such as surgical instruments, implants, and prosthetics.

In conclusion, aluminium alloy is a versatile material that has a wide range of applications due to its lightweight, strength, corrosion-resistant, and other useful properties. Its use has enabled the production of more efficient, durable, and cost-effective products in various industries.

1.3. TYPES OF ALUMINIUM

Cast aluminium alloys and wrought aluminium alloys are the two main divisions of aluminium alloys. Compared to wrought aluminium alloys, which have fewer than 4% alloying elements, cast aluminium alloys have more than 22%. Mechanical properties are significantly impacted by the ratio of alloying elements. When more alloying elements are introduced, Aluminium lacks its ductility, rendering most cast alloys vulnerable to brittle fracture. By keeping ductility and other desirable features, wrought alloys have allowed researchers to increase the strength, resistance to corrosion, conductivity, and other attributes of aluminium. The preponderance of aluminium items, such as those created by extrusion or rolling, are composed of wrought aluminium [7]. Various types of wrought aluminum alloys can be classified based on the presence of certain elements

such as copper, manganese, silicon, magnesium, combinations of magnesium and silicon, zinc, and lithium.

1.4. WROUGHT ALUMINIUM GRADES

Wrought aluminum alloys are those that are shaped by rolling, forging, or extruding in their solid form. There are many different grades of wrought aluminium alloys, each with its own unique set of properties and applications [8]. Here are some of the most common wrought aluminium grades:

- **1000 series:** This series is pure aluminium and has excellent corrosion resistance, electrical conductivity, and thermal conductivity. It is often used in chemical processing equipment, reflectors, and electrical conductors.
- **2000 series:** This series contains copper as the main alloying element and has good strength and fatigue resistance. It is used in aircraft and aerospace applications, as well as in military and defence equipment.
- **3000 series:** This series contains manganese as the main alloying element and has good formability, corrosion resistance, and weldability. It is used in heat exchangers, cooking utensils, and pressure vessels.
- **4000 series:** The 4A01 series of aluminum plates, which fall under the 4000 series, are characterized by their high silicon content. These plates are commonly used as building materials, forging materials for mechanical parts, and welding materials. With a silicon content typically ranging between 4.5% and 6.0%, they exhibit a low melting point, excellent corrosion resistance, as well as heat and wear resistance.
- **5000 series:** This series contains magnesium as the main alloying element and has good strength, formability, and corrosion resistance. It is used in marine and automotive applications, as well as in structural components.
- **6000 series:** The primary alloying elements in this series are magnesium and silicon, leading to advantageous properties such as strength, weldability, and resistance to corrosion. It is used in architectural and structural applications, as well as in the production of consumer goods.
- **7000 series:** This series contains zinc as the main alloying element and has the highest strength of all the wrought aluminium grades. It is used in aircraft and aerospace applications, as well as in sports equipment.

- **8000 series:** Comprising a diverse range of alloying elements, these alloys serve various purposes such as achieving high-temperature performance, reduced densities, enhanced stiffness, and other unique characteristics. Primarily utilized in helicopter parts and other space applications, these alloys offer exceptional properties to meet the specific requirements of these industries.

In conclusion, wrought aluminium alloys offer a wide range of properties and applications due to their different compositions. The selection of the appropriate grade of aluminium alloy depends on the specific requirements of the application, such as strength, corrosion resistance, and formability.

1.5. WELDING OF ALUMINIUM

When combining comparable or dissimilar materials, welding creates a localized, permanent bond with or without the use of heat, pressure, or just pressure. The process can be performed with or without the utilization of filler material. Compared to welding steel or iron, welding aluminium is different [9]. Users may anticipate a number of challenges due to the unusual composition of aluminium, including hot cracking, porosity, and thermal conductivity. There are several ways to weld aluminium, including:

1. Tungsten inert gas welding
2. Metal inert gas welding
3. Gas welding
4. Laser welding
5. Friction stir welding

- **Tungsten inert gas (TIG) welding:**

TIG welding is commonly used in industries that require high-quality, precise welds, such as aerospace, automotive, and medical equipment manufacturing. This is a popular method of welding aluminium, in which an electrode heats the metal to create a weld. The welding process is precise and clean, producing a high-quality weld with minimal distortion.

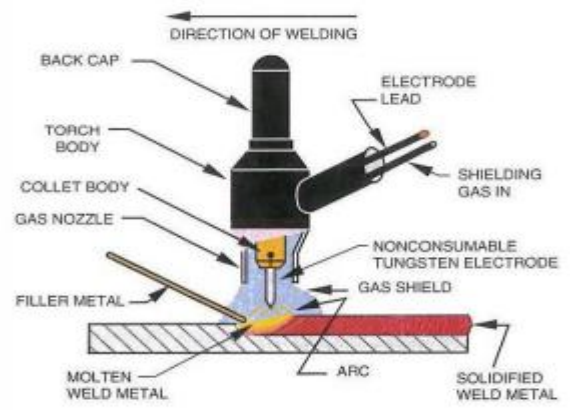

Figure 1.1: Schematic diagram of TIG welding [10]

- **Metal inert gas (MIG) welding:**

Metal Inert Gas (MIG) welding, also known as Gas Metal Arc Welding (GMAW), is a welding method that utilizes a wire electrode and shielding gas to join two metal components through fusion. In this process, a continuous wire electrode is fed through a welding gun, simultaneously delivering the shielding gas to safeguard the weld pool against atmospheric impurities. By generating an electric arc between the wire and the workpiece, the metal is heated, melted, and subsequently solidifies to create a robust bond. Notably faster than TIG welding, MIG welding enables the production of sturdy welds with minimal exertion.

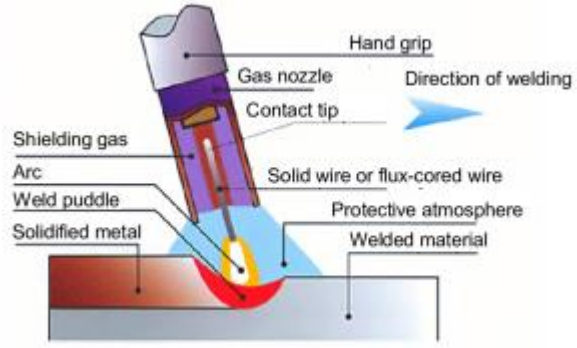

Figure 1.2: Schematic diagram of MIG welding [10]

- **Gas welding:**

Gas welding is a welding technique in which the joining of two metal parts is achieved by utilizing a flame generated through the combustion of fuel gas and oxygen. The process involves heating the metal parts to a temperature high enough to melt and fuse them together. Gas welding can be performed using several types of fuel gases, including acetylene, propane, and natural gas, and requires a welding torch equipped with a tip that mixes the fuel gas and oxygen. This method uses a flame to heat the

metal and then a filler rod is added to create a weld. Gas welding is a versatile method of welding and can be used on a wide range of aluminium thicknesses.

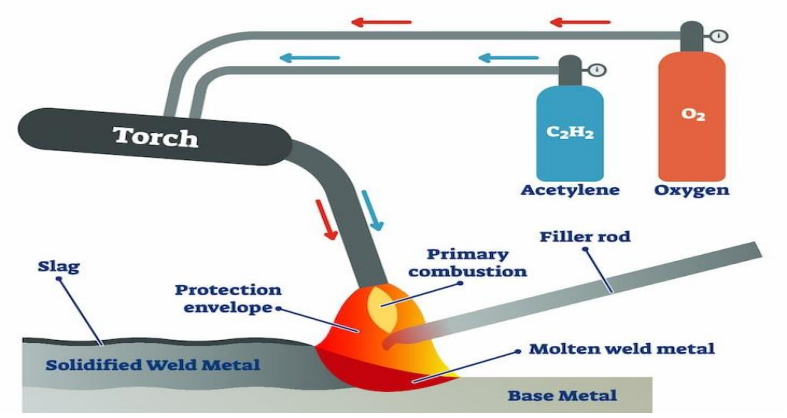

Figure 1.3: Schematic diagram of gas welding [10]

- **Laser welding:**

Laser welding is a welding method that employs a high-intensity laser beam to effectively combine two metal parts. By generating a concentrated heat source, the laser beam melts and joins the metal parts together through fusion. Laser welding finds widespread application in industries that demand exceptional precision and accuracy, including aerospace, medical equipment manufacturing, and electronics sectors. It is also used in automotive manufacturing and jewelry making. Laser welding is a precise method of welding, which produces a high-quality weld with minimal distortion.

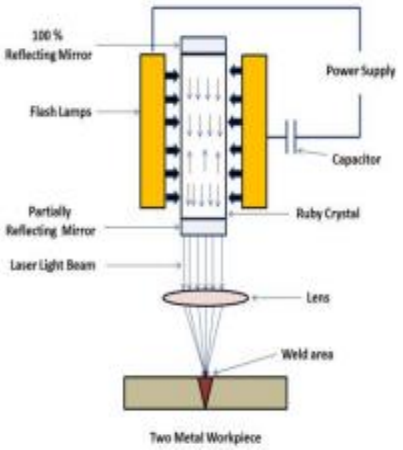

Figure 1.4: Schematic diagram of LBW [11]

- **Friction-stir welding:**

This method uses a rotating tool to create friction and heat, which softens the metal and creates a weld. Friction stir welding is a relatively new method of welding, but it

is increasingly being used to weld aluminium due to its advantages such as producing high-quality welds with minimal distortion.

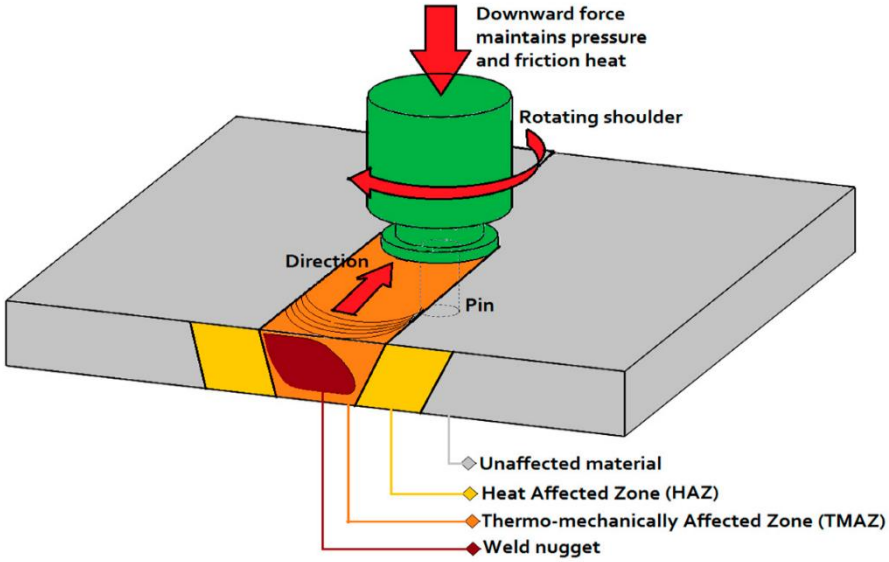

Figure 1.5: Schematic diagram of FSW [12]

Every one of these methods possesses distinct advantages and disadvantages, and the selection of the appropriate method will hinge upon the specific requirements of the project.

- **Cold Metal Transfer (CMT):**

The fundamental feature of this method is an extremely steady arc with very little heat input. The MT welding method allows users to attain optimal settings while combining various materials, during welding when a short circuit is detected, the digital process control detaches the droplet by retracting the wire, as soon as a short circuit develops, the wire travels forward and is pulled back. As a consequence, during the arc-burning phase, the arc only generates heat for a relatively brief time. The arc length is detected and calibrated mechanically. In this process, no matter how rapidly the operator welds or how rough the work piece's surface is, the arc remains stable. The above discussion leads to the conclusion that CMT is highly useful for welding everywhere.

CHAPTER 2

LITERATURE REVIEW

2.1. INTRODUCTION

Aluminum alloys play a crucial role in various industries due to their desirable properties, including lightweight, corrosion resistance, and high strength-to-weight ratio. It is widely utilized in the automotive, aerospace, and marine industries. To enhance the weldability and mechanical properties of aluminum alloys, filler materials and activated flux are commonly employed during the welding process.

This section provides an overview of the relevant literature pertaining to dissimilar materials joints, encompassing joints between different alloys or metals, diverse joint types such as lap and butt joints, and varying thicknesses of joints where different sheet thicknesses are welded together. It also includes the use of activated fluxes with different joining methods. The literature review focuses on research papers published within the past 15 years to ensure an up-to-date understanding of the advancements in welding using different joining techniques. By thoroughly examining the literature, this review aims to identify any existing research gaps and establish the objectives of the current work.

Table 2.1: Summary of literature review studied by various researchers

Author	**Process**	**Material & Filler wire**	**Activating Flux**	**Process Parameters**	**Results**
Kun Liu et. al. 2022 [13]	CMT	5A06 Al plate Al ER5087 (Al-Mg4.5) wire of diameter 1.2 mm	SiC	Shielding gas - Argon (99.99%) Gas flow- 18L/min Travel speed- 0.5m/min Wire feed- 6.5m/min	1. Without flux • UTS= 260 MPa • YS= 110 MPa 2. With flux • UTS= 325 MPa • YS= 135 MPa 3. Tensile strength of MMC increased by increasing SiC content. 4. Ductility decreases as we increase SiC content.

Huaqing Lai et.al. 2014 [14]	CMT	5052 Al alloy and Galvanized Q235 steel sheet ER4043 filler wire	Plumbum (Pb) foil	Shielding gas – Pure Argon Gas flow – 15L/min Welding speed – 600 mm/min Wire feed – 3.6-4.3 m/min	• Without - 120 MPa • With – 167 MPa Flux improves the wettability of molten metal.
Y. Ruan et.al. 2012 [15]	Twin-wire MIG	6082-T6 Al alloy plate of thickness 6mm ER5087 filler wire	SiO_2	Voltage (V) Former wire – 19-21 Rear wire –20-22 Current (A) Former wire – 210-220 A Rear wire – 150-160 A Weld speed – 120 cm/min	• Using the flux, there is slight increase in the width of the HAZ. Also, there is an increment in depth of penetration of about 26% and the main reason for this increase is arc constriction and higher arc temperature.
Yiming Huang, et.al. 2022 [16]	Laser welding	5083 Aluminium alloy of size 100*50*2 mm^3 ER5356 wire of dia 1.2 mm	Cr_2O_3	Laser power – 1.5 kW Weld speed – 3-6 mm/s Wire Feed – 0-4 mm/s Gas flow – 15 L/min	• Full penetration at laser power of 1.5 kW. In active laser welding, the maximum tensile strength of 255 MPa was recorded while in active laser wire filling welding, the max tensile strength of 275 MPa was recorded.
K.R. Madavi et.al. 2021 [17]	MIG	SS316 plate of 5 mm thickness	ZnO Al_2O_3 SiO_2	Voltage – 20-28V Current – 170-210 Shielding Gas – Ar + CO_2 Weld speed – 140 mm/min	• With the use of activating flux, 20.62% higher penetration is obtained. • For flux welding, there is 10.8% increase in UTS and about 15% increase in productivity

				Gas Flow – 12L/min	which reduces the welding time
Abhishek Chakraborty et.al. 2021 [18]	MIG	SS-202 plate of 6.15 mm thickness	Ammonium Ferro-Sulphate, Sodium Bi-Carbonate, Ammonium Carbonate	Voltage – 220 V Current – 100 A Load – 20 kgf	• Maximum depth of penetration achieved is 2.81 mm which is 66% more than that in without flux.
Anand Baghel et.al. 2021 [19]	MIG	AISI 1018 plate of 6 mm	$Al_2(SO_4)_3$, NaOH, Na_2CO_3, $NaHCO_3$, Borax	Voltage – 210 V Feed rate – 3.5 mm/sec Weld speed – 10 mm/sec Gas flow – 5 L/min	• With the use of Borax flux, there is an increase of DOP of about 43%. • And the aspect ratio (width/depth) is also getting reduced in fusion zone.
Her-Yueh Huang 2010 [20]	MIG	AISI 1020 carbon steel of thickness 5 mm. Carbon steel wire (ER70S-6) of diameter 1.6 mm.	Fe_2O_3 SiO_2 $MgCO_3$	Voltage – 20.2-23.3 V Current – 180-220 A Speed – 346-454 mm/min Joint gap – 0-2 mm Shielding gas – Argon Flow – 15 L/min	• Taguchi method is used to find process parameters and L9 orthogonal array is used. • The use of these fluxes increases the DOP and enhances the mechanical properties and hardness. • In case of $MgCO_3$ flux, there is maximum tensile strength of joint which is about 24% more than that of without flux.
D.K. Dwivedi et.al. 2017 [21]	A-TIG M-Tig	409 Ferritic Stainless Steel of thickness 8 mm	SiO_2 for A-TIG SUPERTIG ER309L for M-TIG	Current – 230 & 125 A Speed – 80 mm/min Voltage – 15 & 12.7 V	• With the use of A-TIG process, there was an increase in joint penetration and the mechanical properties were also enhanced and

				Shielding gas – Argon with 10 L/min	more than that of M-TIG process. • The toughness in A-TIG process is low in FZ but they were improved using post weld heat treatment.
Anand Baghel et. al. 2021 [22]	TIG	SS202 and SS304 plates of thickness 3 mm.	$CaCl_2$ Fe_2O_3	Current – 80 A Feed rate – 3.5 mm/sec Weld speed – 10 mm/sec Gas flow – 5 l/min	• Oxide flux increases the depth of penetration but the chloride flux decreases it. • The hardness of fine grain HAZ is more than that of coarse grain HAZ.
Her-Yueh Huang et.al. [23]	GTAW	Austenitic stainless steel (SS304) 5mm thick	MnO_2 and ZnO in the ratio (80:20)	Current – 125 A Speed – 75 mm/min Arc length –3mm Gas – ($Ar+N_2$) (N_2- 2.5-10 vol% Flow - 20µL/min	• There was increase in DOP and weld area as we add more N_2 in shielding gas. • It also enhanced the tensile properties and hardness and reduced the angular distortion of welded joint.
A. Kulkarni et.al. 2017 [24]	A-TIG	316 SS and P91 (9Cr1Mo) martensitic steel plates of 8 mm thickness	Multi-component flux TiO_2 (35%) SiO_2 (40%) NiO (15%) CuO (10%)	Current – 230 A Voltage – 14-16 Speed - 80±2 mm/min Arc length –3mm Shielding Gas – pure Argon Flow- 10 L/min	• The welded joint was free from defects like crack, porosity, lack of penetration, etc. • There was increase in hardness from 316L to P91 side and maximum hardness observed in P91 steel. • But the tensile test results are not good. UTS was lower than that of parent metals.

R. Mohanraj et.al. 2020 [25]	Flux assisted GTAW	SS304 and SS316 L of dimension 300x150x6 mm	Al_2O_3 CuO	Current – 120-150 A Voltage –16-18V Gas – Ar(18 l/m) Travel speed – 3.5 mm/min	• More hardness was recorded in case of Al_2O_3 flux assisted welding. • Presence of Al_2O_3 flux produces closely packed structure in weld region. • Also, the specimen formed using Al_2O_3 flux had more strength than that used CuO flux. •
R. S. Vidyarthy et.al. 2020 [26]	TIG	Mild steel plate of thickness 8 mm	SiO_2 TiO_2 CuO MoO_3 Cr_2O_3	Current – 220 A Speed – 80 mm/min Arc length –3mm	• The maximum depth of penetration occurred is 5.5 mm with the use of SiO_2. • There was significant increase in hardness also. In FZ, hardness is 215 HV which is more than 1.5 times that of base material. In HAZ, the hardness achieved is about 173 HV which is also more than hardness of base material.
M.Vasudevan et.al. 2017 [27]	TIG	1.BOP on 9 mm thick 304 & 316 SS plates. 2.Sq-butt joint on - 10 mm thick 304 SS plate - 12 mm thick 316 SS plate Using multi component flux in single pass	Cr_2O_3, TiO_2, SiO_2, Fe_2O_3 NaF, CaF_2 And multi component flux	Current – 100 A Voltage –13-14V Required quantity of flux for welding was 200 mg/m.	• There were no such differences in microstructure of weld produced with and with flux. • The aspect ratio (D/W) is less in case of single component flux, that's why multi component flux is used.

					• There was also increase in toughness with the use of activated flux.
Darko Bajic et.al. 2018 [28]	PAW	6 mm thick 316L SS	BC31-solder	Current – 158 A Voltage – 28.6V Speed – 16 cm/min	• The tensile strength enhances by using activating flux. • Also, the elongation of the base metal is more than the welded joint.
Z. D. Zhang And Q. J. Cao 2012 [29]	MIG	AZ61 magnesium alloy plate of 6 mm thickness, AZ61 magnesium alloy wire of 1.6 mm dia as filler wire	KCl, TiO_2, $CaCl_2$	Shielding gas- Ar Voltage – 23 V Weld speed – 0.6 m/min Feed rate – 9 m/min Gas flow – 17 L/min	• With KCl flux, the welding current is more than the average current, and there is reduced droplet size and metal transfer period which leads to less spatter. •
k. Devendranath Ramkumar et.al. 2015 [30]	TIG	5 mm thick plate of Inconel 718	SiO_2 TiO_2	Voltage – 9-12 V Current – 140A Electrode dia – 3.2 mm Gas – Argon Flow – 19 lpm Weld Speed – 110 mm/min	• The DOP increases as we increase the welding current and both the fluxes resulted in full penetration while employing 140A current. • The UTS increases in TiO_2 flux joint but decreases in SiO_2 flux assisted joint as compared to base metal. • There was also increase in hardness for both flux assisted weldments.
Dixit Patel et.al. 2022 [31]	FATIG	Hastelloy C-22 plate of thickness 6 mm	SiO_2 Al_2O_3 Fe_2O_3 CuO	Current - 200A Arc length– 3mm Welding speed – 170 mm/min	• Penetration enhancement was due to variations in peak temperature and arc voltage.

			mix with acetone	Shielding gas - Argon (15 l/min)	• Acidic flux produces smoother weld surface and gave more DOP and D/W ratio. • SiO_2 reduces weld bead width up to 25%.
Ashish kumar Nath et.al. 2021 [32]	Laser beam welding	Pure Titanium rectangular strip of 2 mm thickness	MgF_2	Laser power – 2.15 kW Speed – 4 m/min Gas – Argon Flow – 10 L/min	• With the use of active flux, there were improvements in tensile strength and ductility. • Also, the peak temperature recorded was high and colling rate was slower in case of welding with active flux.
N. Rakesh, et.al. 2023 [33]	TIG				• Reverse Marangoni convection was responsible for the improvement in penetration. • Effective fluxes mainly oxides, chlorides and fluorides were effective during A-TIG process. • Flux coated filler wire shows better penetration results.
Jay J. Vora, et.al. 2021 [34]	Arc and Beam welding				• Oxide fluxes were effective for both welding. • Use of flux increase penetration but reduces weld width. • More scope of flux use is there in MIG, PAW, and EBW.

2.1. LITERATURE SUMMARY

The discussion encompasses an array of welding processes, their corresponding process parameters, combinations of welding materials, as well as the mechanical and microstructural analyses conducted by different researchers on welded joints. The concluding points drawn from the literature review are:

- The Cold Metal Transfer (CMT) process highlights the notable importance of the retractive movement of the filler wire during the short-circuit phase. This movement effectively minimizes spatter formation, thereby eliminating the need for post-weld machining and facilitating the production of welds with superior quality.
- The optimal process parameters mainly depend on material, filler wire metal, type of activated flux, and other surrounding conditions.
- By augmenting the wire feed rate and reducing the welding speed, it is possible to achieve a higher heat input, resulting in a weld bead characterized by enhanced penetration.
- The use of activated flux not only increases the depth of penetration but also enhances the mechanical properties.

2.2. RESEARCH GAPS

On the basis of literature review the following research gap have been identified:

- The investigation into the joining of thin aluminium alloy sheets is considerably limited, necessitating further exploration in this field.
- Limited research work is carried out in CMT process using activated flux
- Idea to improve wettability in molten pool by employing different active fluxes has not been studied much.
- Use of different activated fluxes and its effect with varying welding parameters is also found to be missing.

2.3. OBJECTIVE OF WORK

- Fabrication of weld bead samples of AA6082 with and without flux using Cold Metal Transfer Process.
- Optimization of process parameters to study the weld on bead of AA6082 by using Cold Metal Transfer (CMT) welding process.
- To study the effect of activated flux on weld bead geometry, microstructure and mechanical properties.

CHAPTER 3

EXPERIMENTAL WORK AND METHODOLOGY

3.1 MATERIAL SELECTION

3.1.1 Aluminium AA6082

AA6082 is widely recognized as a Structural alloy and boasts the highest strength of all the 6000 series aluminium alloys. Its composition primarily consists of silicon and manganese. Not only is it renowned for its exceptional machining capabilities, but it also exhibits remarkable properties such as weldability, cold machinability, and corrosion resistance. The high manganese content enables it to control its grain structure, resulting in a stronger alloy that is particularly useful for applications demanding additional strength and toughness.

3.1.2 ER4043

ER4043 is a type of aluminium welding wire that is commonly used in the Gas Tungsten Arc Welding (GTAW) and Gas Metal Arc Welding (GMAW) processes. It is a silicon-based wire that is typically used for welding aluminium alloys containing silicon, such as 6XXX series alloys. ER4043 is known for its excellent welding characteristics, including its ease of use, low spatter, and good fluidity. It is also well-suited for welding thin gauge materials and has good colour match with the base material. Additionally, ER4043 is a versatile wire that can be used for both welding and brazing applications.

3.2 COMPOSITION

Chemical composition of filler materials (wt.%) and substrate materials in accordance with ASTM E 1251:2011 as shown in Table 3.1.

Table 3.1: Base plate and filler metal chemical composition (wt%)

Composition	Si	Fe	Zn	Cu	Ti	Mg	Mn	Cr	Al
AA6082	0.8	0.5	0.2	0.1	0.1	0.7	0.5	0.25	Bal
ER4043	5.6	0.8	0.10	0.3	0.02	0.05	0.05	0.05	Bal

3.3 APPLICATIONS OF AA6082

AA6082 aluminium alloy is commonly used in various applications that require a high strength-to-weight ratio, good machinability, and resistance to corrosion [35]. Some of the typical applications of AA6082 include:

1. Structural components in the aerospace industry, such as aircraft wings and fuselage.
2. Automotive industry, such as body panels, wheels, and chassis components.
3. Marine industry, such as boat hulls, masts, and fittings.
4. Construction industry, such as scaffolding, ladders, and bridges.
5. Sports equipment, such as bicycle frames and components, and tennis racquets.
6. Electrical components, such as electrical enclosures and conductors.
7. Packaging industry, such as cans and containers for food and beverage products.
8. Medical equipment, such as surgical instruments and equipment due to its non-toxic and non-magnetic properties.

Overall, AA6082 is a versatile alloy that can be used in a wide range of applications where high strength, durability, and corrosion resistance are required.

3.4 SAMPLE SIZE

The aluminium alloy AA6082 plate of specification 100 mm X 60 mm X 3 mm is used and the filler wire diameter is 1.2 mm. As per the study conducted by researchers it has been concluded that welding of Aluminium alloys depends upon various parameters like welding current, heat input, shielding gas, voltage, filler material and welding speed.

3.5 DEVELOPMENT OF CMT WELDING SYSTEM

The development of CMT (Cold Metal Transfer) welding system involves the use of a welding technique that combines high welding speeds and low heat input to achieve precise and consistent welds. The CMT process involves feeding a consumable electrode wire into a weld pool at a low current level, which creates a short circuit. The current is then increased, causing the wire to detach and create a small droplet that transfers to the workpiece [36]. This process is repeated multiple times per second, resulting in a high-speed welding process with minimal heat input. The CMT welding system was developed

to address the limitations of traditional welding processes, such as spatter, distortion, and poor weld quality. By using a controlled short circuit and precise droplet transfer, the CMT process can produce high-quality welds with minimal spatter and distortion [37]. Additionally, the low heat input of the CMT process allows for welding of thinner materials without the risk of warping or burn-through. The development of the CMT welding system has revolutionized the welding industry, allowing for faster, more precise, and higher quality welds in a wide range of applications.

3.5.1 Selection of Process Parameters

After reviewing several literature sources, it has been determined that the quality of a welded joint is largely influenced by the welding electric current, the argon gas flow rate, and the filler material used. As a result, these factors have been selected as process parameters for the current study, and a series of experiments will be conducted using different combinations of these parameters. The Taguchi Design of experiments approach was utilized to carry out the experiments, with varying levels of the factors being tested.

3.5.2 Design of Experiments

The Design of Experiments (DOE) is a statistical tool that helps establish relationships between process variables and output parameters in various fields, including manufacturing and non-manufacturing industries like medicine, engineering, biology, and physics. It was developed by Ronald A. Fisher in the late 1920s when he was conducting agricultural research to improve crop yield, where he introduced a novel approach compared to traditional methods. Fisher documented his findings in a book on DOE, which outlined how to determine the outcome of an experiment based on input factors. In essence, DOE is used to evaluate the cost-effectiveness and process efficiency of a hypothesis.

3.5.3 Taguchi orthogonal array design

The Taguchi orthogonal array design is a statistical technique used in the Design of Experiments (DOE) to efficiently test and optimize multiple parameters with a minimal number of experiments. The approach is named after Dr. Genichi Taguchi, a Japanese engineer who developed the technique in the 1950s.

The Taguchi orthogonal array design involves selecting a set of input variables, or factors, that are hypothesized to affect a specific output, or response. The factors are then assigned specific levels, and an orthogonal array is chosen based on the number of factors and levels. The orthogonal array is a matrix that ensures an equal number of test combinations for each factor level, reducing the number of experiments required to obtain reliable

results. The Taguchi orthogonal array design is particularly useful in industries where product quality and cost efficiency are critical factors. By using this approach, engineers can identify the most important factors that affect the output and determine optimal levels for each factor, leading to improved product quality and reduced production costs.

In general, Taguchi design of experiments consists of the following steps as shown in the table 3.2 below:

Table 3.2 Steps involved in Taguchi design [38]

STEPS	**DESCRIPTION**
BRAINSTORMING	Determine the number of components and levels involved in reaching the process's goal.
DESIGN EXPERIMENTS	Decide the required orthogonal array and the order of the design runs.
RUNNING EXPERIMENTS	Run experiments in random order as possible.
ANALYSING RESULTS	Determine the best design and performance under ideal conditions.

3.6 EXPERIMENTAL SETUP

AA6082 plate of thickness 3 mm as a substrate material and filler wire ER4043 (1.2 mm) is used to perform the weld bead on CMT machine shown in Figure 3.1. Different test runs have been conducted using various combinations of process parameters, with the approach of modifying one parameter while keeping the remaining parameters unchanged. Table 3.3 shows the operating range of process parameters used in this study. Taguchi L9 orthogonal array was selected for design matrix with and without flux, hence total 18 samples (9 samples of without flux and 9 samples with flux) were created using CMT welding process.

Table 3.3: CMT process variables and their levels

Welding Parameters	**Units**	**Symbol**	**Levels**		
			-1	**0**	**1**
Current	A	I	90	100	110
Welding speed	cm/min	S	30	40	50

The CMT machine represents an enhanced iteration of the GMAW machine. In this research, the TPS400i CMT machine (Figure 3.1) is employed, and its detailed technical specifications are outlined in Table 3.5. During CMT welding, the total welding time is significantly reduced compared to conventional techniques. Notably, approximately one-fourth of the overall welding time is allocated to the short-circuit phase, wherein the current reaches its maximum value before decreasing nearly to zero. This distinct characteristic sets CMT welding apart from other methods and contributes to its efficiency and effectiveness. The utilization of advanced technologies such as high-speed digital process control (DPC) and wire buffer in CMT welding leads to significant cost and energy savings, typically ranging from 30% to 40% [39]. By employing a synergic power source, DPC promptly signals the wire buffer to retract the filler wire during the short-circuit phase. This automatic adjustment of the current level effectively reduces the thermal heat input (THI), resulting in several benefits including minimal spatter, negligible distortion, and low dilution. The combination of these factors contributes to enhanced cost-effectiveness and energy efficiency in CMT welding processes [37,40]. In this CMT machine, a direct current electrode positive (DCEP) configuration is employed. In this configuration, the welding torch, which includes the wire electrode, is connected to the positive terminal of the CMT power source, while the base metal (BM) is connected to the negative terminal. This setup is also known as direct current reverse polarity (DCRP).

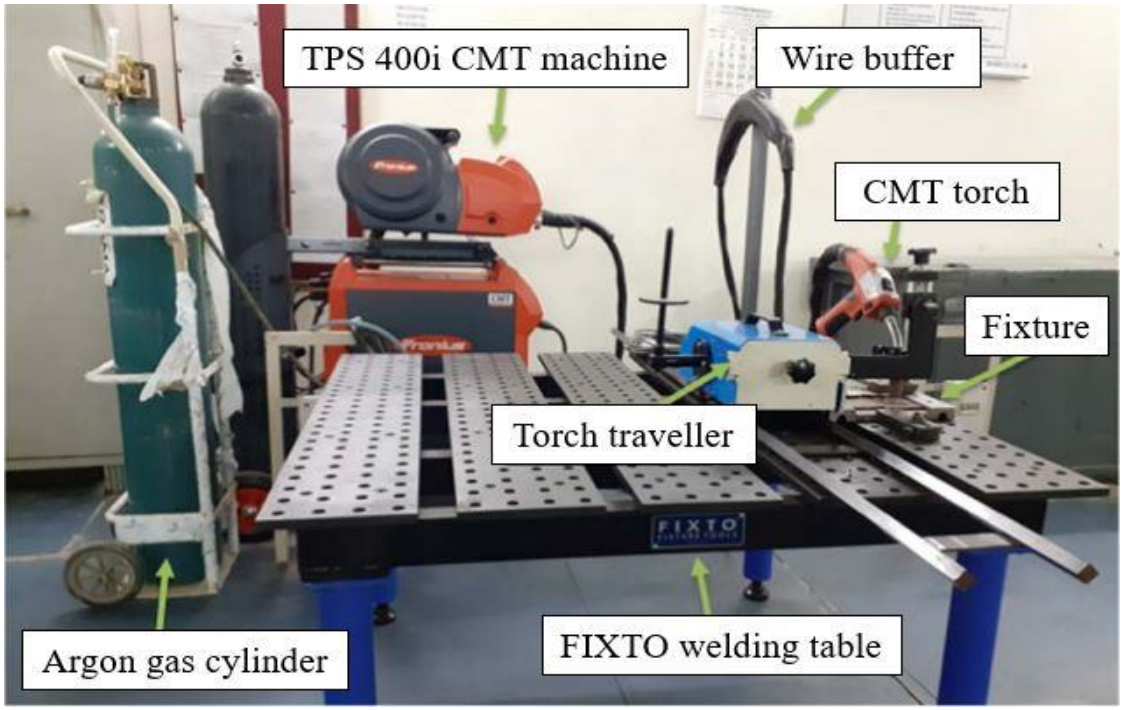

Figure 3.1: Experimental setup of CMT machine

Figure 3.2 illustrates the schematic of a fixture that holds an AA6082. Acetone ($(CH_3)_2CO$) is used to clean each plate before to welding. The surface films and other impurities are then removed from the metal surface using a steel wire brush. The other parameters employed argon (99.99% pure) as the shielding gas, a CTWD of 10mm, a 5mm stick-out, and a 90º torch angle. The conventional bead-on-plate method was employed to lay weld beads on AA6082 plates using a wire with a diameter of approximately 1.2mm composed of ER4043 (AlSi5%).

Table 3.4: Design Matrix

Sample Number	I (A)	S (cm/min)
1.	90	30
2.	90	40
3.	90	50
4.	100	30
5.	100	40
6.	100	50
7.	110	30
8.	110	40
9.	110	50

Table 3.5: Specification of CMT machine

Specifications	Units	Range
Maximum / minimum welding current	A / A	400/3
Welding current / Duty cycle [10 min/40°C]	A / %	400/40
Welding current / Duty cycle [10 min/40°C]	A / %	360/60
Welding current / Duty cycle [10 min/40°C]	A / %	320/100
Operating voltage	V	14.2-34.0
Open circuit voltage (OCV)	V	73
Main's frequency	Hz	50-60
Main's voltage	V	3 x 400
Main's fuse	A	35
Dimension / b	mm	300
Dimension / l	mm	706
Weight	kg	36.45
Degree of protection	-	IP23

The trials, which are conducted in accordance with the design of experiment (DOE) detailed in Table 3.4. In experiments, the Taguchi L9 design matrix is employed to identify the ideal parameters with the number of trials. Table 3.4 displays the results. This technique yields excellent weld bead results, such as high strength, optimal penetration, and a visually appealing appearance, while also minimizing heat-affected zone (HAZ) and substrate material deformation in thin sheets. The dependent parameters for CMT are current, voltage, and wire feed rate, change in one lead to changes in other two.

Before performing welding operation on specimen, AA6082 sheets were cleaned by sand paper to remove the oxide layer. To maintain alignment and spacing, the sheets were positioned on a steel backing bar and secured at the ends using clamps. and then welding operation was performed using argon as a shielding gas by following table experimental arrangement presented in Table 3.4.

After forming the weld bead in plate, then a sample of weld bead is taken out with the help of wire EDM. Then, it was etched using Keller's reagent after being dry polished with 320, 400, 600, 800, 1000, 1200, 1500, 2000, and 2500 grit emery paper.

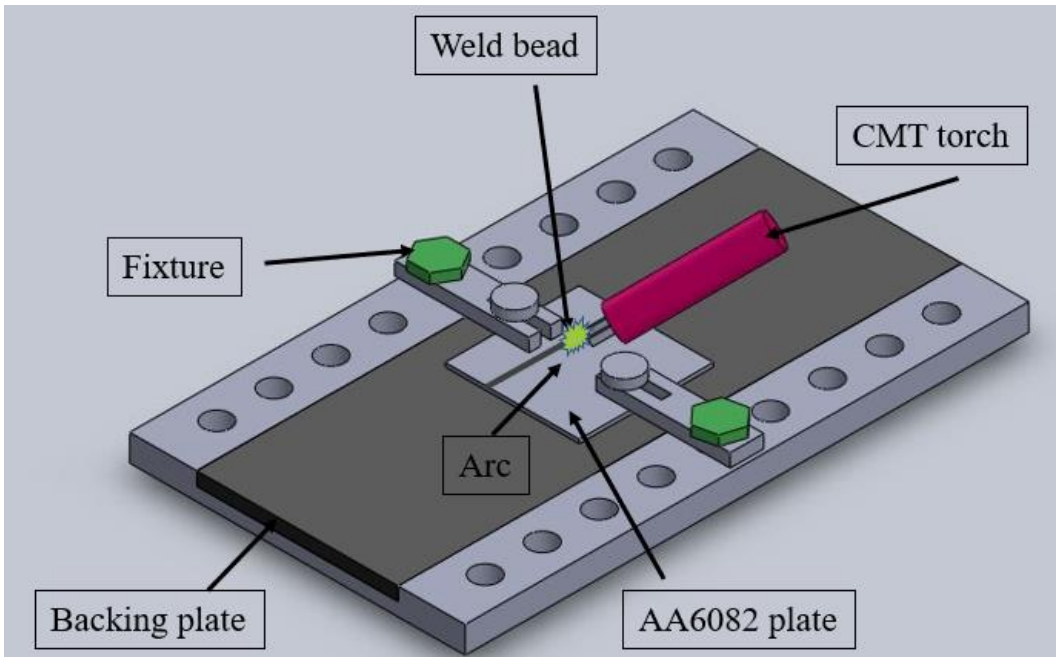

Figure 3.2: Schematic diagram of a fixture holding an AA6082 plate.

3.7 ACTIVATED FLUX

Activated flux is a type of welding flux that contains certain chemical compounds or additives that help to improve the quality of the weld by removing impurities from the surface of the metal being welded. The chemical compounds or additives in the activated flux become active during the welding process, reacting with the oxides and other contaminants on the metal surface and making them easier to remove.

Activated flux is used during welding to improve the quality of the weld and the overall welding process. Some of the main uses of activated flux during welding include:

1. Removal of Oxides and Contaminants: Activated flux contains chemicals that react with oxides and other contaminants on the surface of the metal, allowing them to be easily removed during the welding process. This helps to produce a clean and high-quality weld.
2. Improvement of Wetting: The activated flux can help to improve the wetting of the filler metal on the base metal surface, resulting in a stronger and more reliable weld.
3. Prevention of Porosity: Activated flux can also help to prevent porosity in the weld by eliminating the presence of gases such as hydrogen and nitrogen that can cause porosity.
4. Protection against Oxidation: During welding, the high temperatures and exposure to air can cause the base metal to oxidize. Activated flux can help to prevent oxidation by shielding the weld from the air.
5. Enhancement of Mechanical Properties: Depending on the type of activated flux used, it can also help to enhance the mechanical properties of the weld, such as its strength, ductility, and toughness.

Overall, the use of activated flux can help to improve the quality and reliability of the welding process, leading to stronger and more durable welds.

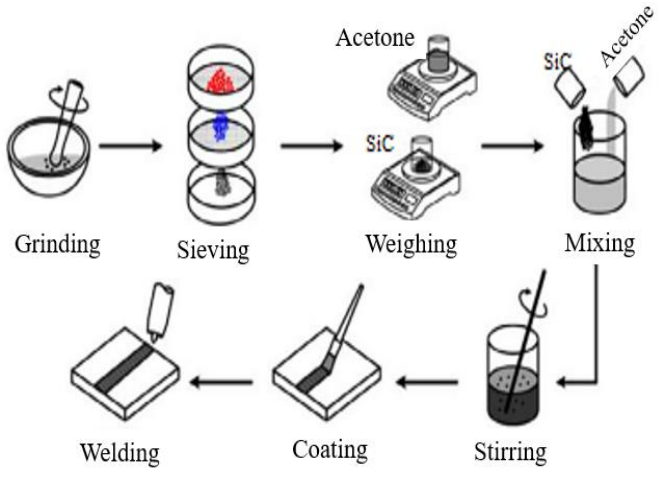

Figure 3.3: Method of applying flux [17]

It is challenging to evenly paste flux that is in powder form over the welding surface. The powder will be combined with acetone and made into a paste for this purpose as shown in Figure 3.3. The SiC flux appears to be evenly distributed on the surface and appears to evaporate easily with acetone.

The base material plate with a thickness of 3 mm was cut into 100*60 pieces for welding trials. And using a paintbrush, flow paste has been placed with a width of 60 mm throughout the full length of the strip. Fluxes boost the arc constriction mechanism and reverse Marangoni effect, which improves penetration. Surface tension gradient turns positive in reverse Marangoni effect, causing molten metal to flow inward as shown in Figure 3.4.

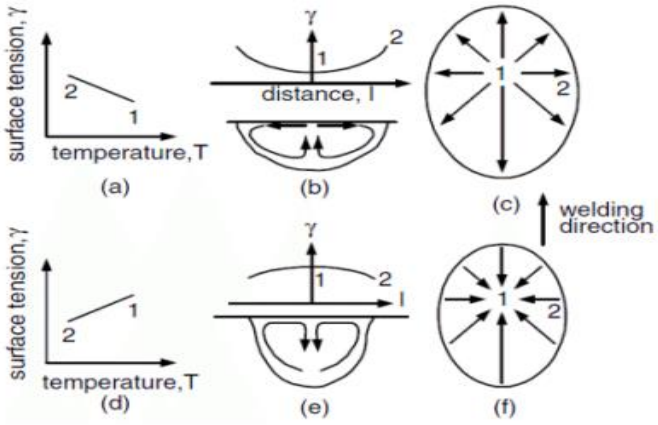

Figure 3.4: Marangoni and Reverse Marangoni effect [22]

3.8 CHARACTERIZATION OF WELD BEAD

Weld bead is the visible result of the fusion process that occurs during welding. It is the metal that has been melted and fused together by the welding process to join two or more pieces of metal. The characteristics of a weld bead are important because they can affect the strength and quality of the welded joint.

3.8.1 Optical Microscope Analysis

The evaluation of optical microscopy was conducted utilizing the Olympus GX41 compact inverted metallurgical microscope, as depicted in Figure 3.6. Detailed technical specifications for this microscope can be found in Table 3.7. The GX41 inverted metallographic microscope is ideally suited for efficient and reliable characterization of specimens, facilitating the examination of metallurgical properties to ensure adherence to production requirements. Its compact and lightweight body enhances portability. The main objective of optical microscopy is to investigate the microstructure of weld bead and get the idea of change in structure of joint at weld bead, heat affected area and parent metal due to welding. The analysis of microstructure provides insights into important features such as grain structure, grain boundaries, and grain size. The primary instrument employed for characterizing the internal grain structure of the metal is the optical microscope. To prepare the samples, a square piece measuring 15 x 10 mm was extracted

from the weld bead. Subsequently, the cross-sectional phase was embedded in an epoxy resin powder using a hot mounting press. The samples were then cooled within the mounting press for a duration of 15-20 minutes.

The cross-sectional surface of the weld bead is subjected to dry polishing using emery paper of various grades, including 100, 320, 400, 600, 800, 1000, 1200, 1500, 1800, and 2000. Following the dry polishing step, wet polishing is performed using velvet emery paper and alumina powder. The samples are then dried using a hot air blower. For revealing the microstructure of AA6082-T6, Keller's reagent (consisting of 1ml HF, 1.5 ml HCl, 2.5 ml HNO3, and 95 ml of water) is applied to the samples for a duration of 15 seconds. After etching with Keller's reagent, the samples are again dried using a hot air blower and examined under an optical microscope.

Figure 3.5: Polishing of sample by emery paper

Figure 3.6: Olympus PS2 Optical Microscope

Figure 3.7: Samples after polishing

Table 3.6: Specifications of Optical Microscope

Optical System			**UIS2 Optical System (Infinity-corrected)**
Microscope Frame	Reflected/Transmitted		Reflected
	Observation method		BF/KPO*
	Illuminator		-
	Illumination System	Reflected light	30W Halogen or Fibre Light Guide (Light source:100 W)
		Transmitted light	-
	Focus	Motorized/Manual	Manual Revolving Nosepiece Up/Down Movement (Stage Stationary Type)
		Stroke	9 mm
		Resolution/Fine adjustment sensitivity	Fine Stroke per Rotation 0.2 mm
	Revolving Nosepiece	Manual type	Quadruple for BF
		Motorized type	-
Stage	Stroke		120(X)x78(Y) mm
Observation Tube	Standard Field (Field number 18)	Inverted Image	Tilting Binocular Observation Tube
	Standard Field (Field number 20)	Inverted Image	Binocular/Trinocular/Tilting Binocular Observation Tube
	Wide Field (Field number 22)	Inverted Image	Binocular/Trinocular/Tilting Binocular Observation Tube
		Erect Image	-
Weight			10 kg
Dimensions			236(W) x 624(D) x 407(H) mm

3.8.2 Penetration (P)

The penetration of the weld bead is the depth to which the weld has melted into the base metal. This is an important characteristic because it affects the strength of the weld joint. Activated flux is a type of welding flux that is designed to increase the effectiveness of a welding process. It is usually added to the weld metal to improve the weld penetration and increase the efficiency of the welding process.

The use of activated flux in welding can have a significant effect on the penetration of the weld bead. Activated flux helps to increase the heat input into the weld, which in turn can increase the depth of the weld penetration. This is because the flux helps to increase the heat transfer rate between the welding arc and the workpiece, allowing the weld to penetrate deeper into the base metal.

3.8.2 Microhardness

Micro hardness testing, also referred to as micro-indentation hardness testing, is a method of evaluating the hardness of a material on a small scale. The technique involves using a precise diamond indenter to create an impression on the material at loads that range from a few grams to one kilogram. By measuring the length of the resulting impression under a microscope, along with the applied test load, a hardness value can be calculated. These hardness values serve as useful indicators of the material's properties and its anticipated durability in service.

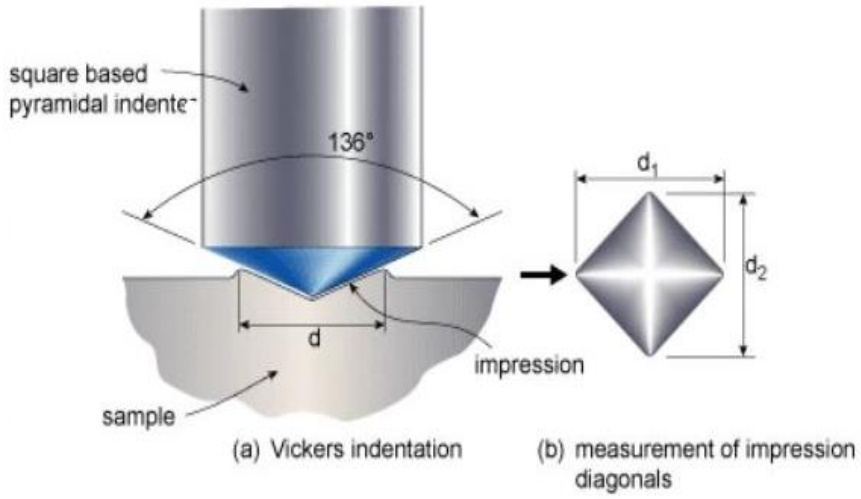

Figure 3.8: Vickers hardness testing machine indenter [41]

To conduct a hardness test, the DRAMIN-40 STRUERS machine utilizes Vickers hardness testing. This method involves using a Vickers indenter, as depicted in Figure 3.8, to apply controlled force to the surface of the material. The resulting pyramid-shaped

indentation is then measured with a microscope to determine the material's hardness value based on the diagonal length of the impression.

The Vickers hardness test was conducted with a 300-gram load and a 10-second indentation dwell time. When a load is applied to a material, it causes the indenter's shape to penetrate the surface, resulting in permanent deformation. The Vickers hardness test is conducted under controlled conditions, with the pressure being monitored for a specific time segment (typically 20 seconds of dwell time). A square-shaped diamond indenter is used for this test. The resulting diagonal length of the indentation on the material's surface is measured, and the Vickers hardness value is calculated using a formula. Figure 3.9 displays the DRAMIN-40 STRUERS Vickers hardness testing machine used for the test. To ensure accurate measurement, the surface is polished to facilitate clear visibility of the indenter's diagonal, as depicted in Figure 3.10.

Figure 3.9: DRAMIN-40 STRUERS hardness testing machine

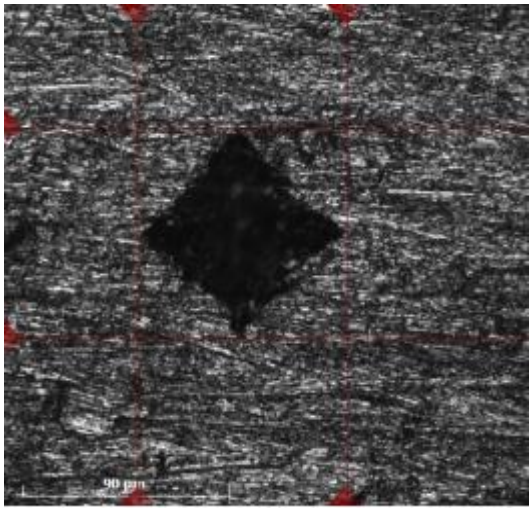

Figure 3.10: Microhardness indentation on aluminium sample.

Table 3.7: Specifications of Microhardness Testing Machine

Model	**Duramin-40 M1**
Loads and Applications	
Load Range (Main Loads)	10 gf – 10 kgf
Knoop Capability	Yes
Brinell Capability	Yes
Vickers Capability	Yes
Stages and Turrets	
XY-stage	Manual
XY-stage stroke, max (mm)	25 x 25
XY-stage or anvil size (mm)	90 x 90
Throat depth (mm)	170
Vertical capacity (mm)	172
Motorized Z-axis	Yes
Motorized turret	Yes
Turret positions	6
Machine weight	101 kg
Anti-collision protection	Yes
Camera and Optics	
Evaluation camera resolution	18 MP
Stage illumination	Yes
Auto illumination	Yes
Laser or LED guider	Yes
Interfaces and Connectivity	
Communication Ports	HDMI, VGA, RJ45, WLAN, USB, RS232
Operation	Embedded Windows 10 PC with 15-inch touch screen.
Bluetooth	Optional
Wi-Fi	Yes

CHAPTER 4

RESULTS AND DISCUSSION

4.1. INTRODUCTION

By examining the bead on the plate, a thorough assessment of the welded bead's geometry can be obtained, encompassing crucial parameters such as weld reinforcement (R), weld penetration (P), and weld width (W). These parameters are visually presented in Figure 4.1, providing a comprehensive overview of the bead's characteristics. Measuring the dimensions of the weld bead is crucial to gain a better understanding of its geometry, which in turn helps to optimize the overall cost of the welding process. To achieve a weld joint that is both effective and economical, it is essential to strive for increased penetration to enhance tensile strength while minimizing the heat-affected zone (HAZ), weld width, and weld reinforcement. By minimizing the consumption of filler wire, cost-effectiveness can be further optimized. [42]. The shaded region "A" in this diagram represents the area of reinforcement, while "B" represents the area of penetration. Dilution is determined by the ratio of the molten base metal (BM) area to the overall fusion zone (FZ) area, or it can be expressed as the ratio of the penetrated area (B) to the total weld metal area (A+B) as shown in equation (1). Dilution plays a critical role as it results in the formation of a new intermediate alloy between the substrate and filler materials, which has a completely different chemical composition than the final weld metal [43-45]. The addition of an appropriate filler material to the base metal (BM) through dilution improves the mechanical properties of the welded bead. Increasing the current and decreasing the welding speed led to an increase in all bead dimensions, as revealed by the study's findings. The calculation of the Weld Penetration Shape Factor (WPSF) is obtained by dividing the bead width (W) by the penetration (P). Similarly, the Weld Reinforcement Form Factor (WRFF) involves determining the ratio between the bead width (W) and the bead height (R). Calculating the heat input using equation (4.2) [46] is crucial in determining the appropriate amount of heat required for materials of varying thickness. The thermal heat input plays a significant role in determining the properties of the weld zone (WM) [47], and greatly influences the cooling rate of the WM. Heat input refers to the quantity of energy transferred per unit length of the weld, and by employing more

efficient techniques to reduce heat input, it is possible to achieve a weld with increased strength. [48].

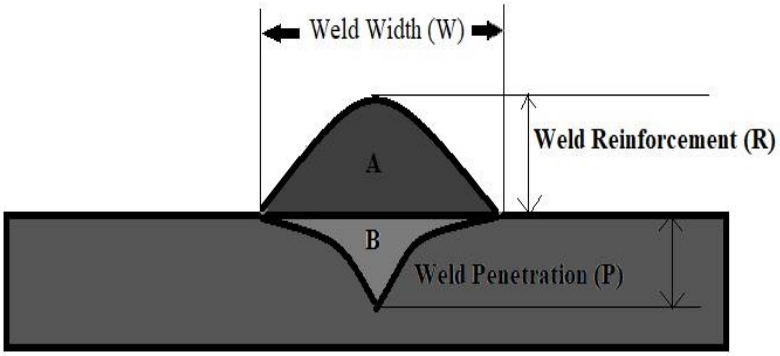

Figure 4.1: Weld Bead Geometry

$$Dilution\ (D)\ =\ \frac{Area\ (B)}{Area\ (A+B)} \qquad (4.1)$$

$$Heat\ input\ (HI)\ =\ \eta\frac{V*I}{S} \qquad (4.2)$$

The variables Q, V, I, S, and η represent the heat input (J/mm), voltage (V), current (A), welding speed (mm/sec), and efficiency (%) respectively. Welding typically has a thermal efficiency of around 80%, according to studies [49,50].

4.2. OPTIMIZATION OF PROCESS PARAMETERS

The Taguchi technique and ANOVA were employed in the design and analysis of experiments, with the assistance of Minitab software. The user-friendly interface of Minitab and its useful features made it convenient to obtain the desired results [51]. The Taguchi technique is an experimental method that reduces the number of required tests in comparison to traditional methods, resulting in an expected model that identifies the most suitable process parameters.

Optimization of process parameters such as current and welding speed during welding involves finding the best combination of these parameters to achieve the desired dilution ratio and weld quality [52].

The current is the amount of electrical energy flowing through the welding arc, which affects the temperature and heat input of the weld. Higher current generally results in higher heat input and faster welding speeds, but may also increase the risk of defects such as porosity and cracking.

Welding speed, on the other hand, affects the rate at which the weld is deposited and the heat input per unit length of the weld. Faster welding speeds can reduce the amount of heat input, but may also reduce penetration and increase the risk of incomplete fusion.

In order to enhance the welding process parameters, a systematic approach like Design of Experiments (DOE) or Response Surface Methodology (RSM) can be employed. These methods entail controlled variation of process parameters and analysis of the resulting welds to identify the optimal conditions that fulfill the desired specifications for dilution and weld quality.

The present study utilized the Taguchi L9 orthogonal array to conduct experiments. For welding samples with each filler wire, a separate L9 orthogonal array was generated with 2 factors (welding current, and filler rod diameter) and 3 levels for each factor. The response variables were dilution (%) and micro-hardness of each welded joint. The Taguchi method was employed with a larger-is-better S/N ratio characteristic. The Taguchi technique was also used to determine the rank of each parameter that influences the microhardness and dilution (%).

4.2.1 Analysis of Variance (ANOVA)

ANOVA stands for Analysis of Variance, which is a statistical method used to analyse the difference between means of two or more groups. It examines whether there is a significant difference between the means of the groups being compared. ANOVA calculates the variance within and between groups and compares them to determine if the observed differences are statistically significant. ANOVA can be used in various fields such as psychology, biology, economics, and engineering to compare the effects of different treatments or interventions on a specific outcome variable [53]. ANOVA is a powerful tool for data analysis and hypothesis testing, and it is widely used in research studies and experimental designs.

In our study, ANOVA was utilized to determine the impact of individual parameters on the response variable, which are dilution (%) and microhardness. Furthermore, ANOVA can identify the most statistically significant process parameter. The ANOVA table displays the results for the dilution and micro-hardness of the welded joint of AA6082 alloy with and without activated flux.

Table 4.1: L9 orthogonal array for the specimens formed without flux

S. No.	Current (A)	Welding speed (cm/min)	Dilution (%)	Penetration (mm)	Micro-hardness (HV)	Heat input (J/mm)
1.	90	30	56.6	1.83	64.19	164.16
2.	90	40	53.2	1.78	61.27	123.12
3.	90	50	51.3	1.69	57.32	98.496
4.	100	30	63.2	2.11	71.35	185.6
5.	100	40	59.6	2.09	67.43	139.2
6.	100	50	56.73	1.97	58.31	111.36
7.	110	30	68.45	2.52	74.39	206.8
8.	110	40	63.46	2.47	70.11	155.1
9.	110	50	60.41	2.32	65.23	124.08

Table 4.2: L9 orthogonal array for the specimens formed with flux

S. No.	Current (A)	Welding speed (cm/min)	Dilution (%)	Penetration (mm)	Micro-hardness (HV)	Heat input (J/mm)
1.	90	30	60.1	2.13	69.35	164.16
2.	90	40	57.7	2.02	63.23	123.12
3.	90	50	52.9	1.78	58.25	98.496
4.	100	30	67.56	2.53	77.43	185.6
5.	100	40	63.11	2.31	73.63	139.2
6.	100	50	58.76	2.13	69.25	111.36
7.	110	30	72.53	2.91	83.57	206.8
8.	110	40	69.87	2.79	78.81	155.1
9.	110	50	66.78	2.43	72.31	124.08

4.2.2 Optimization of weld beads formed without using flux

As per the Taguchi optimization of weld bead samples formed without using active flux, the best level of process parameters with the largest S/N ratio, which indicates the maximum dilution and hardness [54].

Figure 4.2 and Figure 4.3 shows the S/N ratio curves for dilution and microhardness respectively. ANOVA technique was used to check the adequacy of the model. Table 4.3 shows that the maximum dilution occurs at welding current at level 3 i.e., 110A and travel speed at level 1 i.e., 30 cm/min. Similarly, Table 4.6 shows that the maximum hardness is achieved at current at level 1 i.e., 90A and travel speed at level 3 i.e., 50 cm/min.

The adequacy of the model was assessed using the analysis of variance (ANOVA) technique. Table 4.4 and 4.7 present the ANOVA results for the dilution and microhardness of the weld beads formed without activated flux. The tables present data including sum of squares (SS), degree of freedom (DF), mean square (MS) - which is the ratio of SS and DF - F-value, P-value, and percentage contribution. The F-value signifies the ratio of variation between the factors to the variation within the factors, while the P-value denotes the probability, which should be lower than 0.05. The percentage contribution signifies the impact of independent factors on the responses. Adjusting the value of the factor with the highest percentage contribution will exert a substantial influence on the output response. This emphasizes the sensitivity of that specific factor.

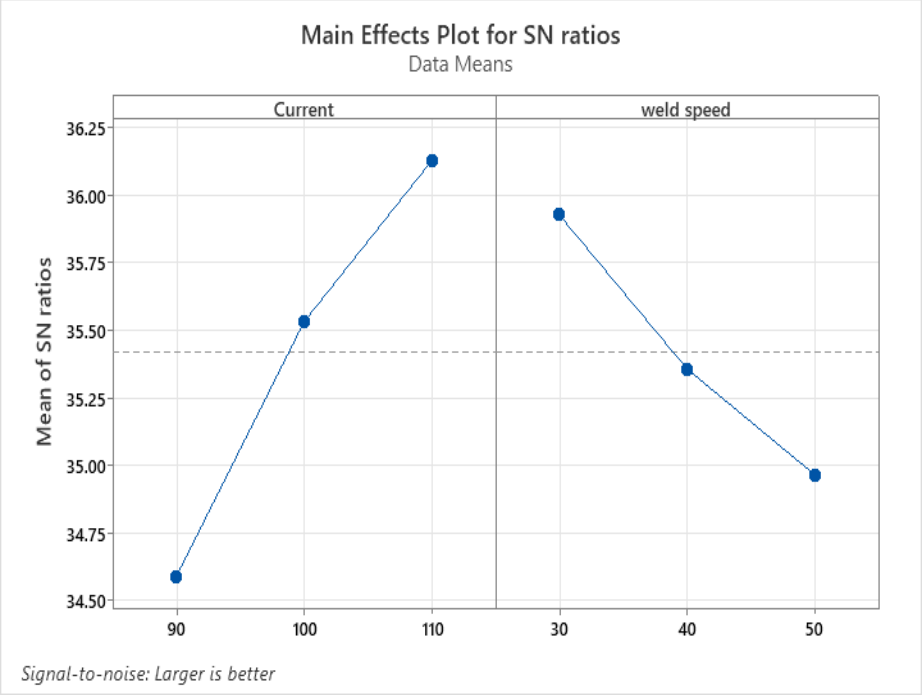

Figure 4.2: Plot between S/N ratio and current, weld speed of WFB for dilution

Table 4.3: Response table of S/N ratio of WFB for Dilution

Level	Welding current	Travel speed
1	34.59	35.93
2	35.53	35.36
3	36.13	34.97
Delta	1.53	0.96
Rank	1	2

Table 4.4: ANOVA table of WFB for Dilution

Source	DF	Contribution	Seq SS	Adj SS	Adj MS	F Value	P Value
Current	2	72.68%	0.000014	0.000014	0.000007	1819.82	0.000
Welding Speed	2	27.24%	0.000005	0.000005	0.000003	681.95	0.000
Error	4	0.08%	0.000000	0.000000	0.000000		
Total	8	100%	0.000019				

Table 4.5: Model Summary of WFB for Transformed Response

S	R-sq	R-sq (adj)	PRESS	R-sq (pred)	BIC
0.0000619	99.92%	99.84%	0.0000001	99.6%	-143.00

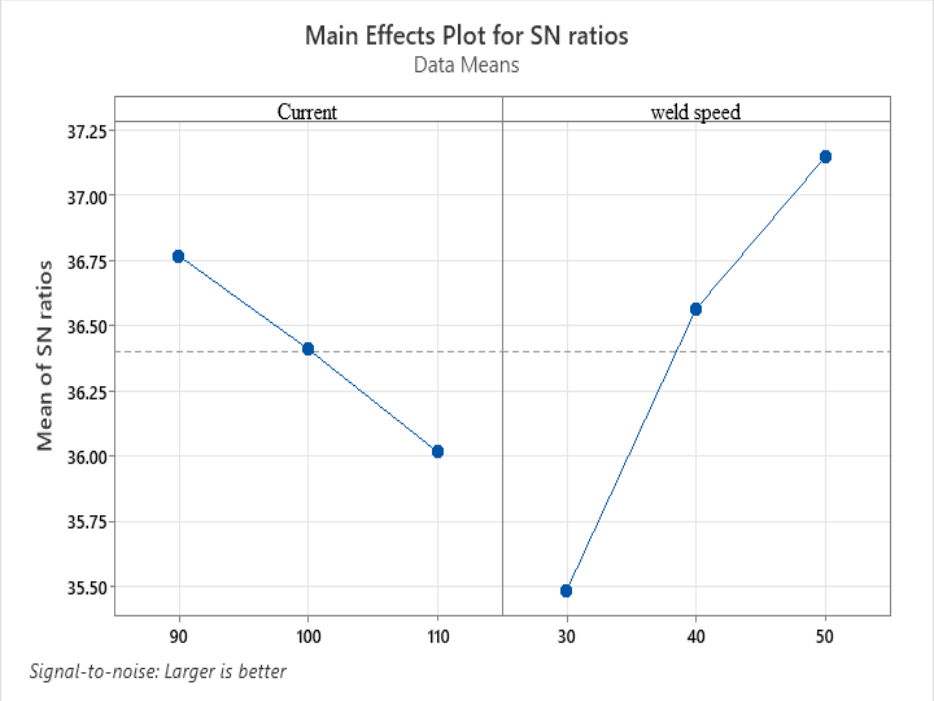

Figure 4.3: Plot between S/N ratio and current, weld speed of WFB for microhardness

Table 4.6: Response table of S/N ratio of WFB for Microhardness

Level	Current	Weld speed
1	36.77	35.49
2	36.41	36.56
3	36.02	37.15
Delta	0.75	1.66
Rank	2	1

Table 4.7: ANOVA table of WFB for Micro-hardness

Source	DF	Contribution	Seq SS	Adj SS	Adj MS	F Value	P Value
Current	2	15.99%	0.000003	0.000003	0.000001	24.34	0.006
Welding speed	2	82.69%	0.000013	0.000013	0.000007	125.84	0.001
Error	4	1.31%	0.00000	0.00000	0.00000		
Total	8	100%	0.000016				

Table 4.8: Model summary of WFB for Transformed Response

S	R-sq	R-sq (adj)	PRESS	R sq (pred)	BIC
0.0002301	98.69%	97.37%	0.0000011	93.35%	-119.36

For dilution, welding current is more dominant (72.68%) as compared to welding speed (27.24%) but for microhardness, welding speed is highly dominant (82.69%) as compared to welding current (15.99%) because of lower P-values and higher F-values. The predicted R^2 values show reasonable agreement with the Adjusted R^2 for all the response parameters, with a difference of less than 0.2. This closeness in values indicates that the majority of data points fall within the regression line. The main distinction between adjusted R^2 and predicted R^2 lies in their interpretations. Adjusted R^2 specifically identifies the independent variables which actually affect the dependent variable, while predicted R^2 assumes that the variation in the dependent variable is explained by each individual variable., providing an indication of the percentage of explained variation. Table 4.5 and 4.8 shows the model summary which indicates R^2 is a validation criterion, which means that in this example the model accounts 99% for dilution and 93.5% for microhardness of the variance in the predictor.

4.2.2 Optimization of weld beads formed using activated flux

As per the Taguchi optimization of weld bead samples obtained using active flux, the best level of process parameters with the largest S/N ratio, which indicates the maximum dilution and hardness. Figure 4.4 and Figure 4.5 shows the S/N ratio curves for dilution and microhardness respectively. ANOVA technique was used to check the adequacy of the model. Table 4.9 shows that the maximum dilution occurs at welding current at level 3 i.e., 110A and travel speed at level 1 i.e., 30 cm/min. Similarly, Table 4.12 shows that the maximum hardness is achieved at current at level 1 i.e., 90A and travel speed at level 3 i.e., 50 cm/min.

The adequacy of the model was assessed using the analysis of variance (ANOVA) technique. Table 4.10 and 4.13 present the ANOVA results for the dilution and microhardness of the weld beads formed without activated flux. The tables present data including sum of squares (SS), degree of freedom (DF), mean square (MS) - which is the ratio of SS and DF - F-value, P-value, and percentage contribution. The F-value signifies the ratio of variation between the factors to the variation within the factors, while the P-value denotes the probability, which should be lower than 0.05. The percentage contribution signifies the impact of independent factors on the responses. Adjusting the value of the factor with the highest percentage contribution will exert a substantial influence on the output response. This emphasizes the sensitivity of that specific factor.

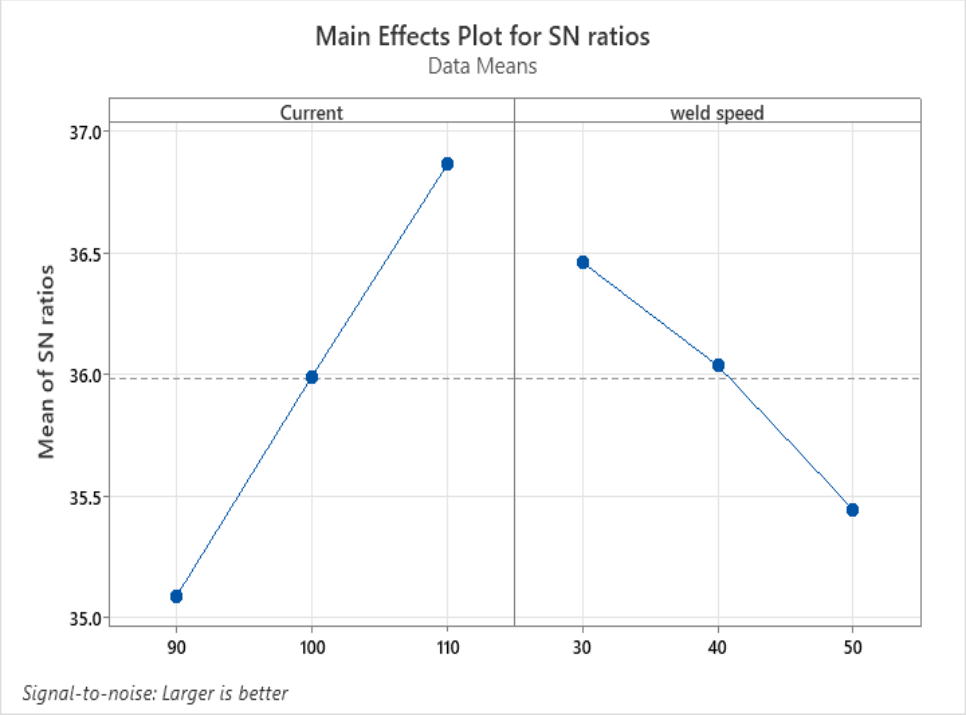

Figure 4.4: Plot between S/N ratio and current, weld speed of FB for dilution

Table 4.9: Response table of S/N ratio of FB for Dilution

Level	Welding current	Travel speed
1	35.09	36.46
2	35.99	36.04
3	36.86	35.45
Delta	1.77	1.01
Rank	1	2

Table 4.10: ANOVA table of FB for Dilution

Source	DF	Contribution	Seq SS	Adj SS	Adj MS	F-value	P-value
Current	2	75.50%	3946778	3946778	1973389	203.88	0.000
Welding Speed	2	23.76%	1241946	1241946	620973	64.16	0.001
Error	4	0.74%	38716	38716	9679		
Total	8	100%	5227440				

Table 4.11: Model summary of FB for Transformed Response

S	R-sq	R-sq (adj)	PRESS	R sq (pred)	BIC
98.3824	99.26%	98.52%	196002	96.25%	114.03

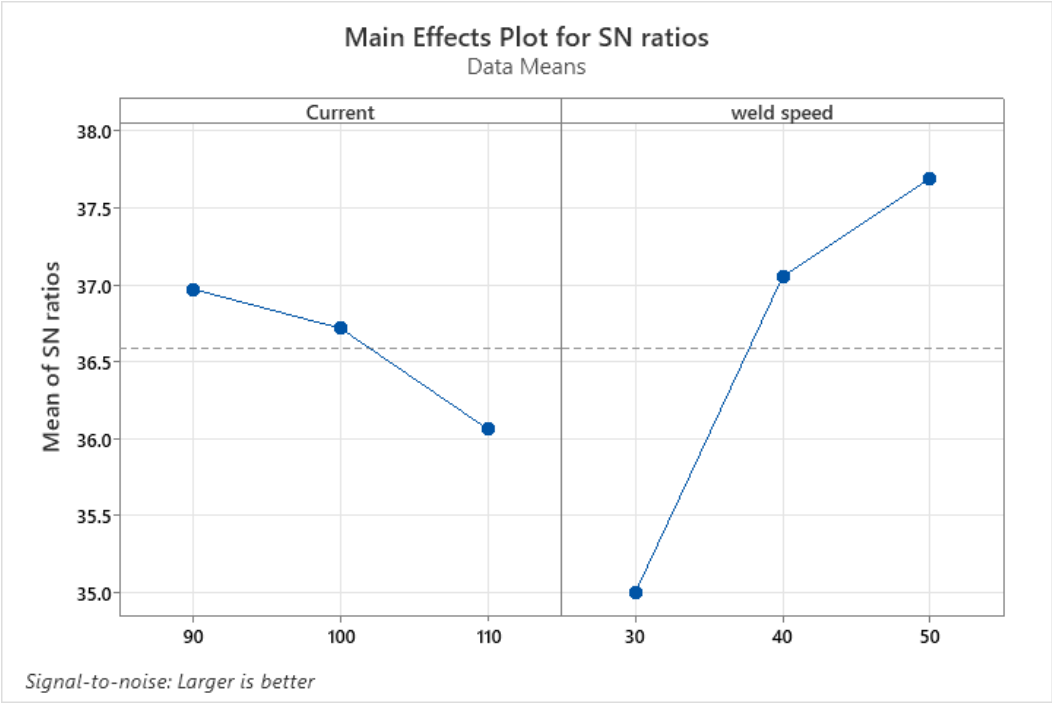

Figure 4.5: Plot between S/N ratio and current, weld speed of FB for microhardness

Table 4.12: Response table of S/N ratio of FB for Microhardness

Level	Current	Welding speed
1	36.97	35.01
2	36.72	37.05
3	36.06	37.69
Delta	0.91	2.68
Rank	2	1

Table 4.13: ANOVA table of FB for Microhardness

Source	DF	Contribution	Seq SS	Adj SS	Adj MS	F-value	P-value
Current	2	10.00%	0.017493	0.017493	0.008746	20.15	0.008
Welding speed	2	89.01%	0.155738	0.155738	0.077869	179.35	0.001
Error	4	0.99%	0.001737	0.001737	0.000434		
Total	8	100.00%	0.174968				

Table 4.14: Model Summary of FB for Transformed Response

S	R^2	R^2 (adj)	PRESS	R^2 (pred)	BIC
0.0208368	99.01%	98.01%	0.0087920	94.98%	-38.25

For dilution, welding current is more dominant (75.50%) as compared to welding speed (23.76%) but for microhardness, welding speed is more dominant (89.01%) as compared to welding current (10.00%) because of lower P-values and higher F-values. The predicted R^2 values show reasonable agreement with the Adjusted R^2 for all the response parameters, with a difference of less than 0.2. This closeness in values indicates that the majority of data points fall within the regression line. The main distinction between adjusted R^2 and predicted R^2 lies in their interpretations. Adjusted R^2 specifically identifies the independent variables which actually affect the dependent variable, while predicted R^2 assumes that the variation in the dependent variable is explained by each individual variable., providing an indication of the percentage of explained variation. Table 4.11 and 4.14 shows the model summary which indicates R^2 is a validation

criterion, which means that in this the model accounts 96.25% for dilution and 94.98% for microhardness of the variance in the predictor.

4.3. MACROSTRUCTURE OF WELD BEAD

The cross-sectional macrostructure of the welded joint provides a clear indication of various features such as the presence of pores, the depth of penetration, reinforcement, HAZ, and base metal (BM). The macro-images of the cross-section of a weld bead generated without and with flux, respectively, are shown in Figure 4.6 and 4.7.

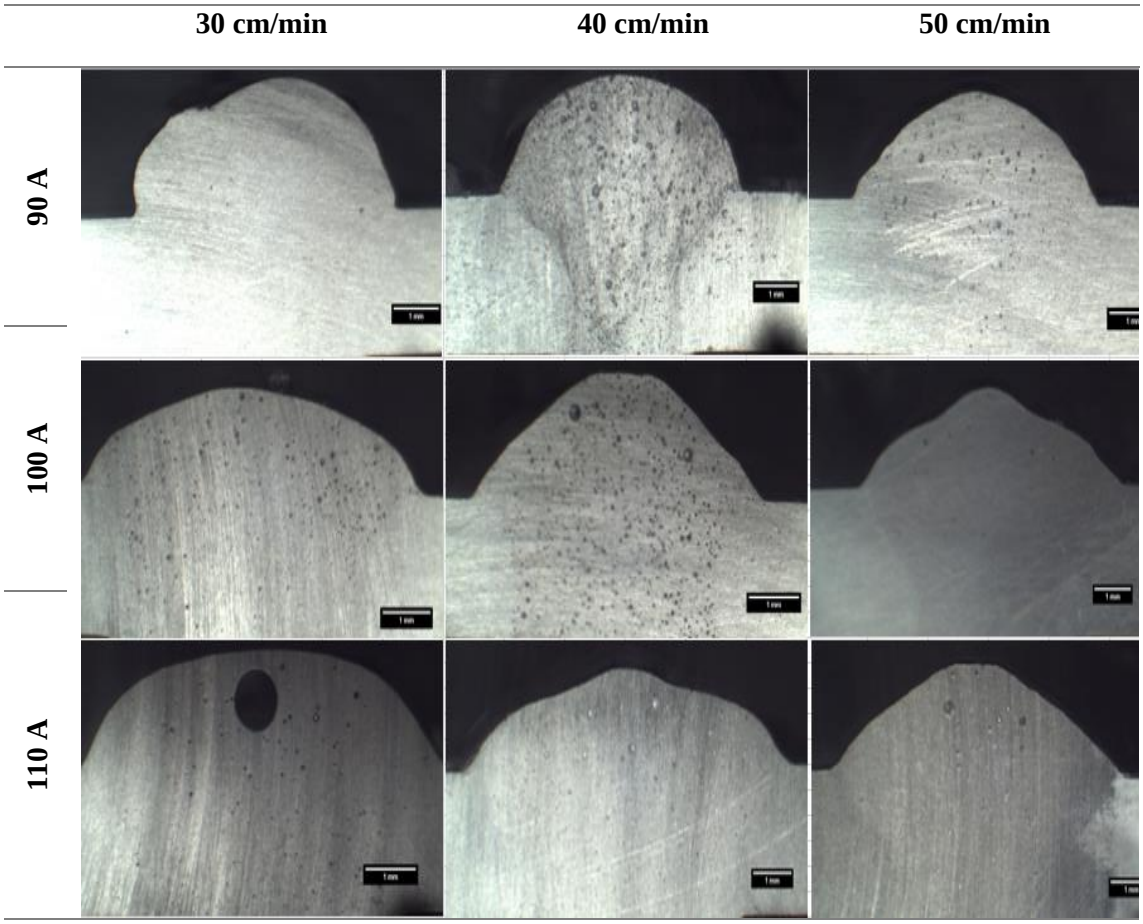

Figure 4.6: Macro-images of weld beads

It can be seen that the weld beads formed using activated flux has a smaller number of pores as compared to those formed without using flux. At elevated heat inputs, aluminium alloys can be prone to the solubility of gases, particularly hydrogen, which leads to the formation of porosity. In addition to heat input, the presence of alloying elements also influences hydrogen solubility. The inclusion of Mg element in aluminium alloys results in a high affinity for hydrogen due to stronger interactions between Mg atoms and hydrogen atoms compared to those between aluminum and hydrogen [55]. Upon polishing and etching of the samples, different welding zones become apparent. The

effect of welding process parameters can be easily seen on the weld bead. Increasing the current while maintaining a constant welding speed leads to an overall increase in weld geometry due to a higher heat input. On the other hand, increasing the welding speed results in reduced penetration, weld width, and dilution due to lower heat input, keeping the current constant.

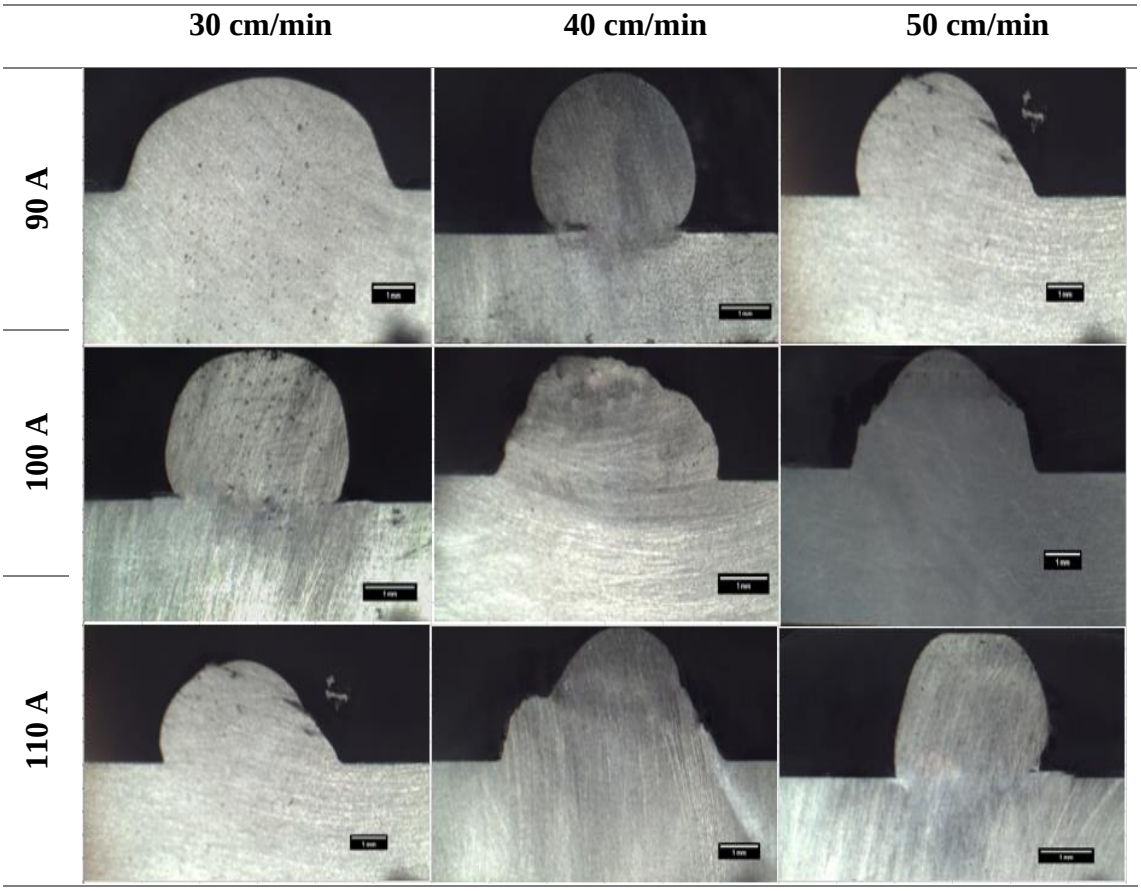

Figure 4.7: Macro-images of weld beads fabricated using flux

4.3.1. Consequences of welding parameters on bead dimension

Process parameters such as welding speed and current exert a significant influence on the geometry of the weld bead, microstructural analysis and mechanical properties. Figure 4.8 demonstrates that, when using the CMT welding technique without flux and keeping the current constant at 100 A, increasing the weld speed from 30 cm/sec to 50 cm/sec results in reduced penetration and decreased weld width, with minimal change in reinforcement height due to low heat input. Similarly, Figure 4.9 indicates that, when keeping the welding speed constant at 50 cm/sec and increasing the current from 90 A to 110 A, with the increase in heat input, the penetration shows a notable initial increase followed by a gradual growth, while the width of the weld gradually increases as well.

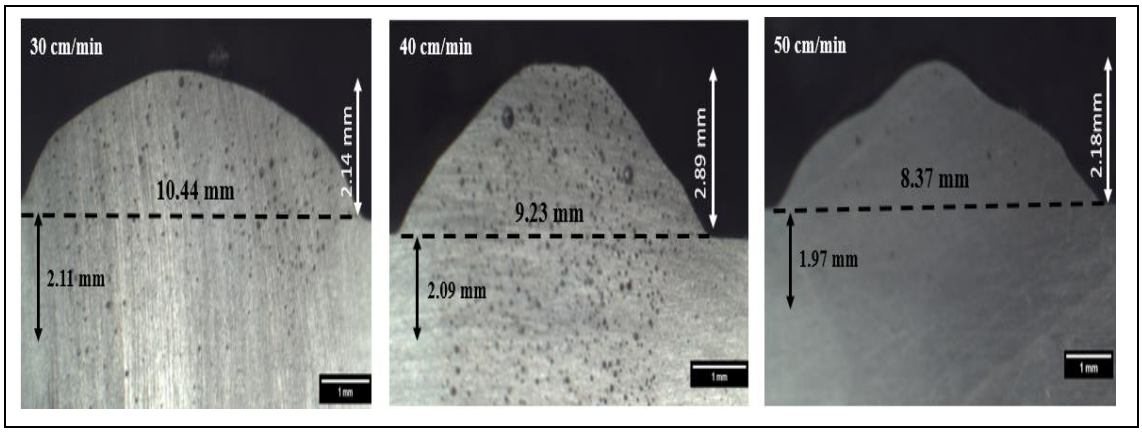

Figure 4.8: Variation in bead geometry for variable welding speeds at constant current of 100 A

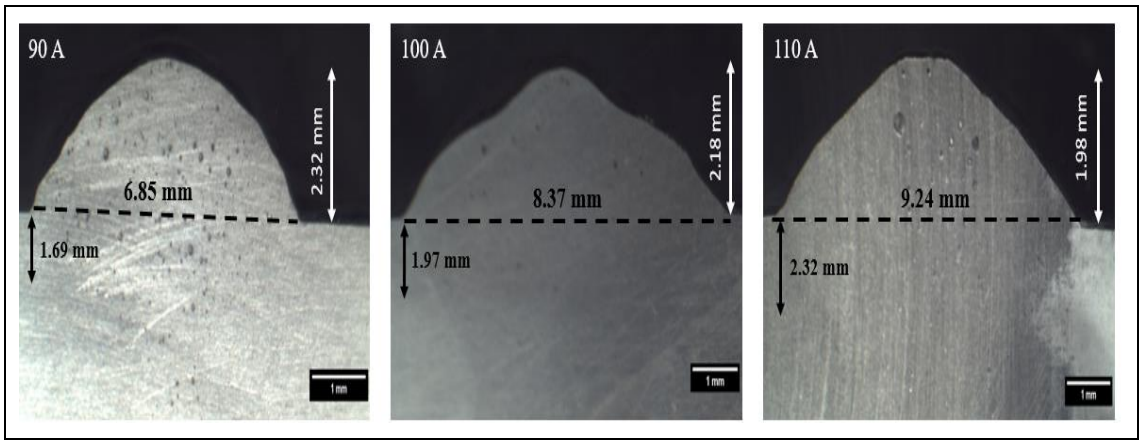

Figure 4.9: Variation in bead geometry for variable current at constant welding speed of 50 cm/min

4.3.2. Consequences of active flux on bead dimension

SiC is utilized as an active flux in this study. The major difference between these two cases is that flux leads to increase in penetration and reduced width. Active fluxes are designed to facilitate better penetration of the weld into the base metal. The active components in the flux can help to reduce surface oxides, improve heat transfer, and enhance the metallurgical interaction between the base metal and the weld metal. These effects can result in deeper penetration of the weld bead into the base metal, leading to increased weld strength and potentially larger dimensions.

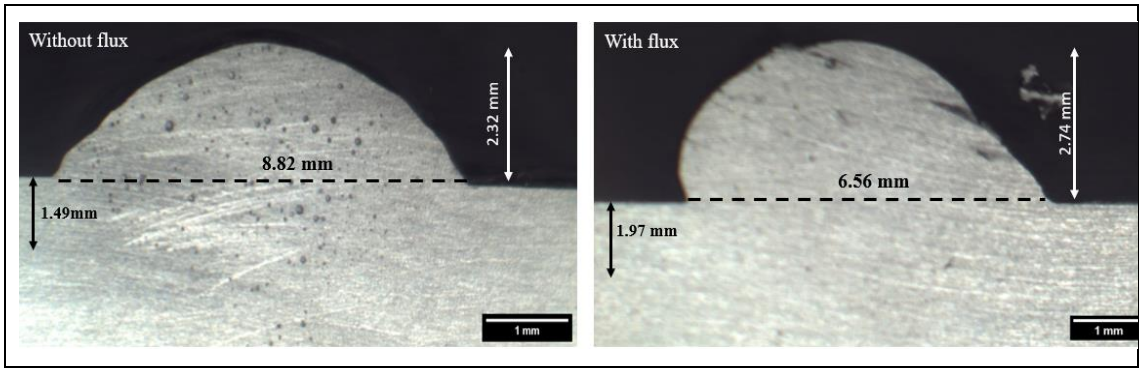

Figure 4.10: Effect of flux on weld bead geometry at constant current and welding speed.

It can be seen from Figure 4.10 that when weld beads fabricated using activated flux and keeping the current and welding speed fixed results in reduced bead width but there is an increase in penetration. There may be an increment in the reinforcement height also. This happens due to presence of active components in the flux can influence the surface tension and fluidity of the molten metal during welding. This altered fluid behaviour can impact the shape and profile of the weld bead.

4.4. MICROSTRUCTURAL ANALYSIS

Images of the microstructure are captured using an Olympus GX41 compact inverted metallurgical microscope. The microstructure of aluminium alloy 6082 is composed of a face-cantered cubic (FCC) aluminium matrix with a mixture of magnesium, silicon, and manganese as the main alloying elements. The presence of magnesium and silicon results in the formation of Mg_2Si and Al_2MgSi particles, which strengthen the material and improve its mechanical properties. These particles are uniformly distributed throughout the aluminium matrix, creating a fine-grained microstructure that enhances the material's strength and toughness. The microstructure of the AA4043 filler wire is primarily composed of an FCC aluminium matrix with a small amount of silicon and magnesium as the main alloying elements [56]. Aluminium alloy 6082 has a fine-grained microstructure composed of an FCC aluminium matrix with Mg_2Si and Al_2MgSi particles, which provides excellent strength, toughness, and corrosion resistance. When welding aluminium alloy 6082, the use of AA4043 filler wire results in a weld with a similar microstructure to the base metal, ensuring excellent mechanical properties and corrosion resistance [57]. When SiC flux is introduced, the silicon carbide particles act as nucleation sites for the formation of new phases during solidification. This leads to refined microstructures with smaller grain sizes in the weld bead. The presence of fine grains can improve the mechanical properties of the weld, such as tensile strength and hardness. Furthermore, SiC flux can alter the morphology and distribution of intermetallic compounds that form in the weld zone. Intermetallic compounds, such as Al-Si and Mg-Si, are typically present in aluminum alloys and can affect the weld's mechanical properties. The addition of SiC flux can help in reducing the size and volume fraction of these intermetallic compounds, leading to improved weld performance. Additionally, the SiC flux can influence the formation of oxide films and their interaction with the molten metal during the welding process. By promoting the removal of oxide films and improving the wetting ability of the filler metal, SiC flux can enhance the overall weldability and reduce defects such as porosity.

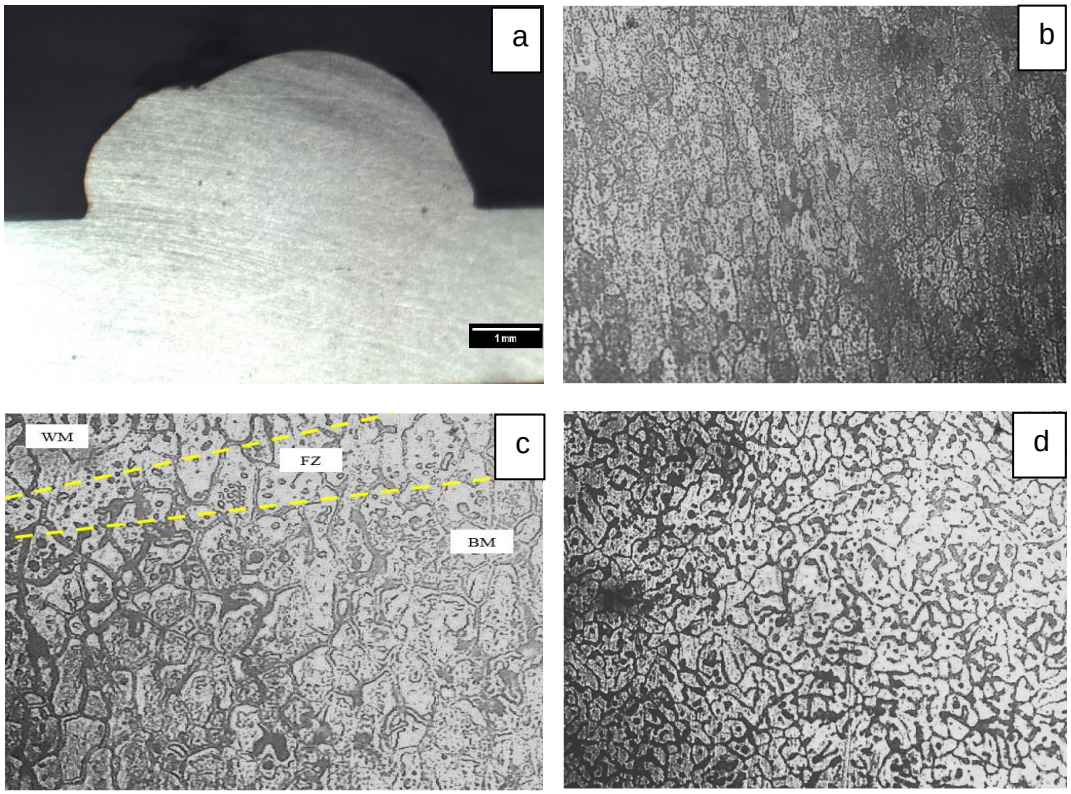

Figure 4.11: (a) WFB at 90 A. Microstructure images at 200 µm (b) BM, (c) FZ (d) WZ

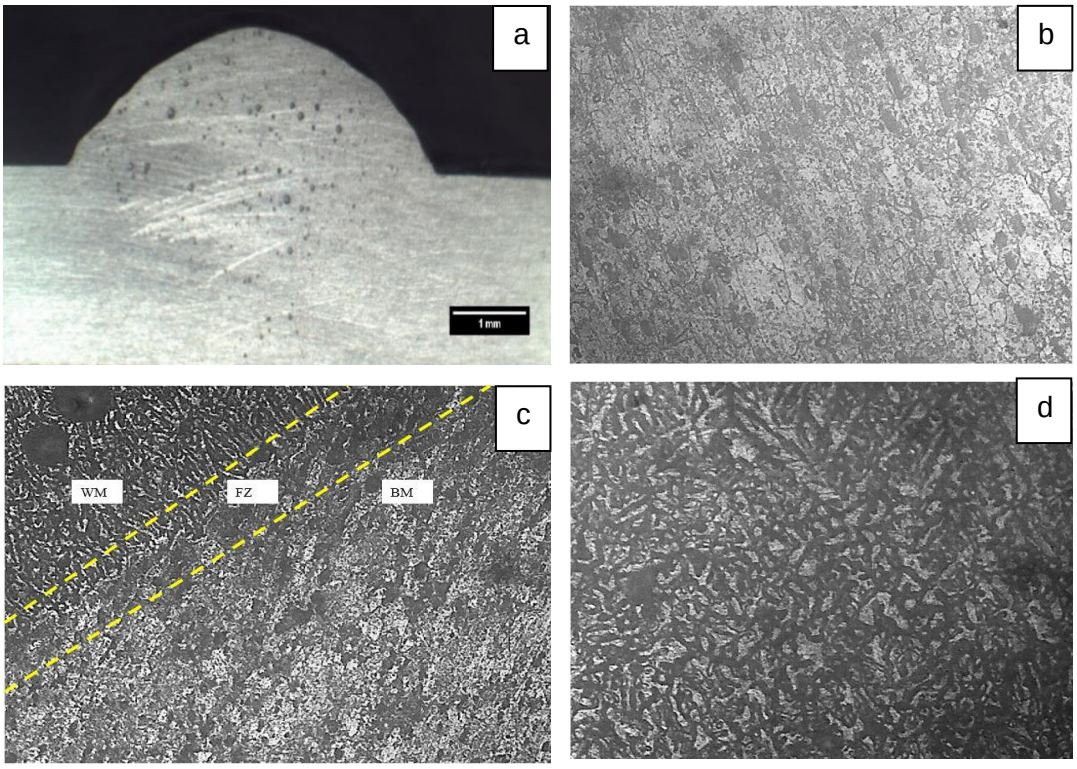

Figure 4.12: (a) WFB at 100 A. Microstructure images at 200 µm (b) BM, (c) FZ (d) WZ

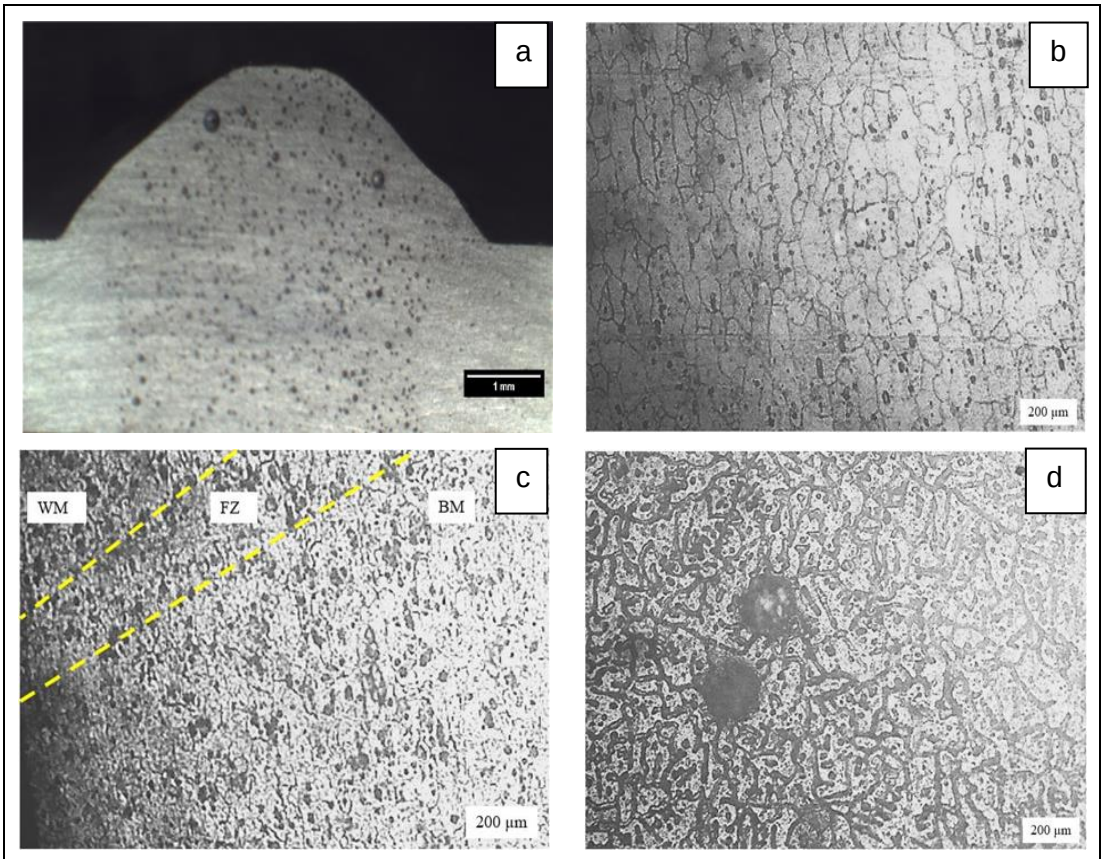

Figure 4.13: (a) WFB at 110 A. Microstructure images at 200 µm (b) BM, (c) FZ (d) WZ

Figure 4.11 to 4.16 shows the microstructural images from optical microscope for the weld beads fabricated using with and without activated flux. A total of six samples were collected to examine the microstructure, three from without using activated flux and other three from those which uses SiC flux. Base Metal (BM), Weld Zone (WZ) and Fusion Zone (FZ) are the places where microstructure is taken. Image (c), which is actually heat affected zone (HAZ), clearly shows the fusion line where AA6082 fuses with ER4043 filler metal. The separation of the source metal and weldment's microstructure by fusion lines (shown by yellow dashes) is evident in Figures 4.11(c), 4.12(c), 4.13(c), 4.14(c), 4.15(c), and 4.16(c). The grain structure and grain boundaries are clearly depicted in Figure 4.11(b), 4.12(b), 4.13(b), 4.14(b), 4.15(c), and 4.16(b), which represent the parent metal. At higher current values (specifically 110 A), a notable presence of black spots is observed in both the parent metal and the bead region, which can be attributed to the elevated heat input. The non-uniform cooling rate caused by this high heat i/p leads to the formation of a higher number of brittle compounds, particularly Mg_2Si, which is manifested as the black spots. In the weld bead's fusion zone (FZ), Mg_2Si dissolves and subsequently precipitates and coarsens the grains [58,59]. Those black spots negatively impact the surface profile and mechanical properties of the bead. Weld bead with layer

of activated flux is showing better microstructures as compared to weld bead without flux and also the smaller number of pores and better bead aesthetics.

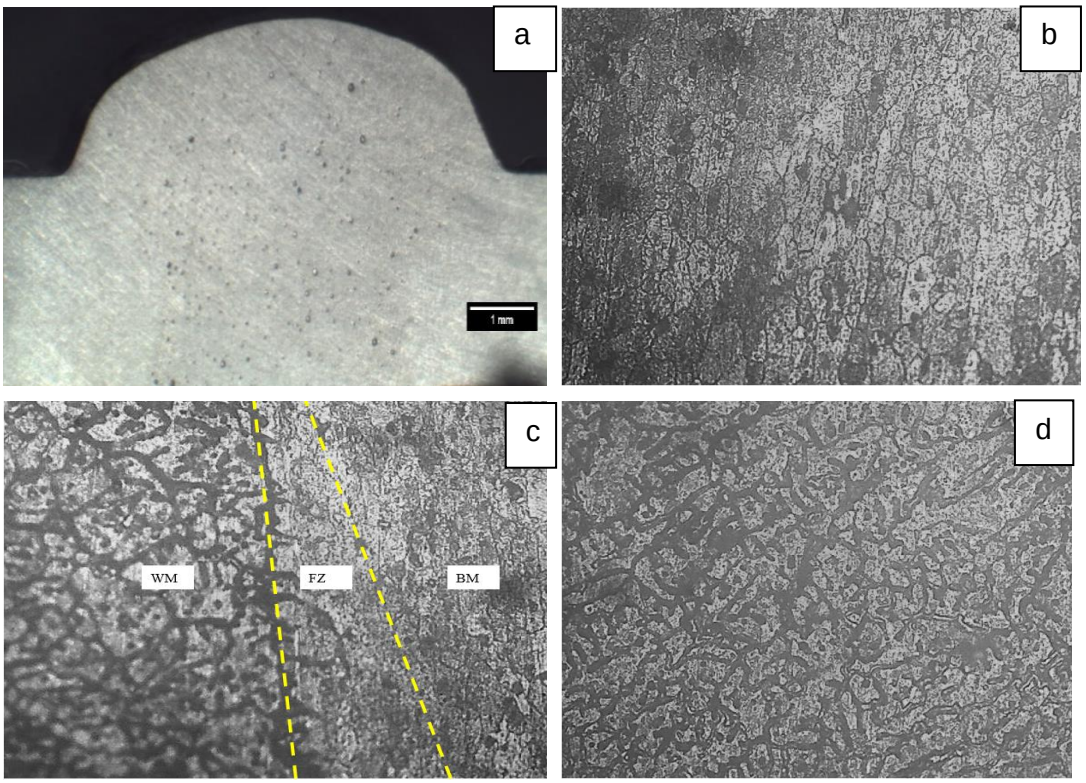

Figure 4.14: (a) FB at 90 A. Microstructure images at 200 µm (b) BM, (c) FZ (d) WZ

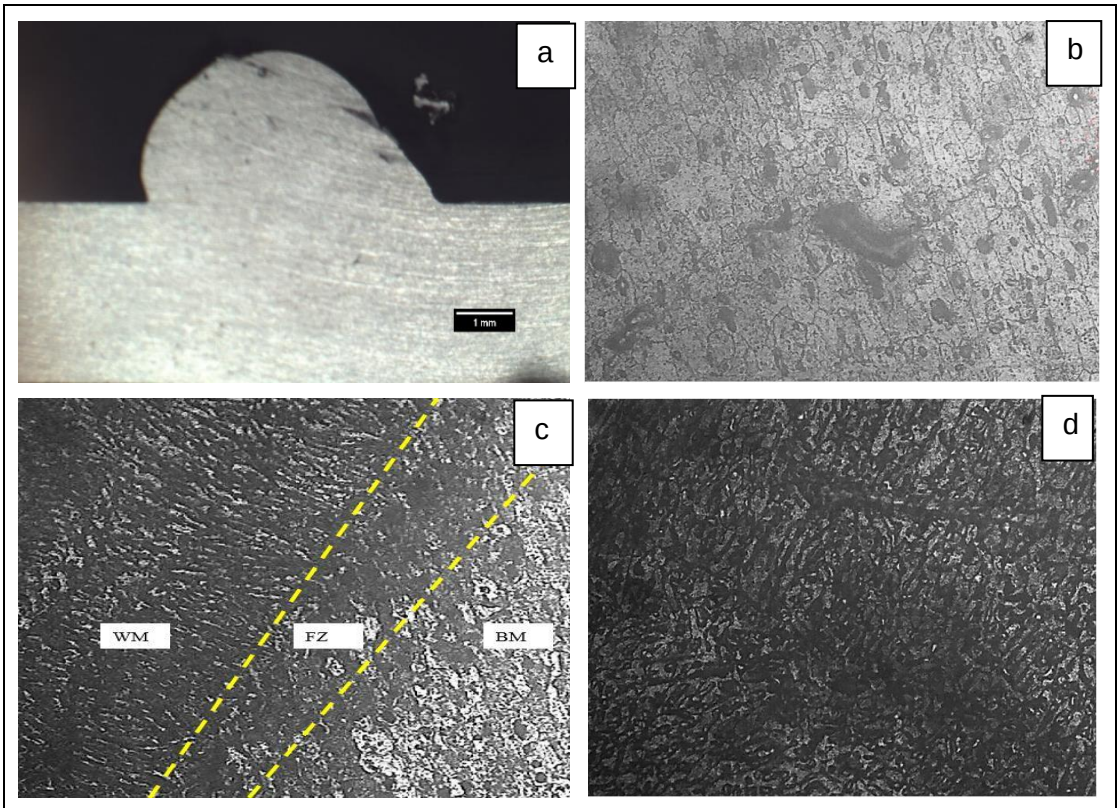

Figure 4.15: (a) FB at 100 A. Microstructure images at 200 µm (b) BM, (c) FZ (d) WZ

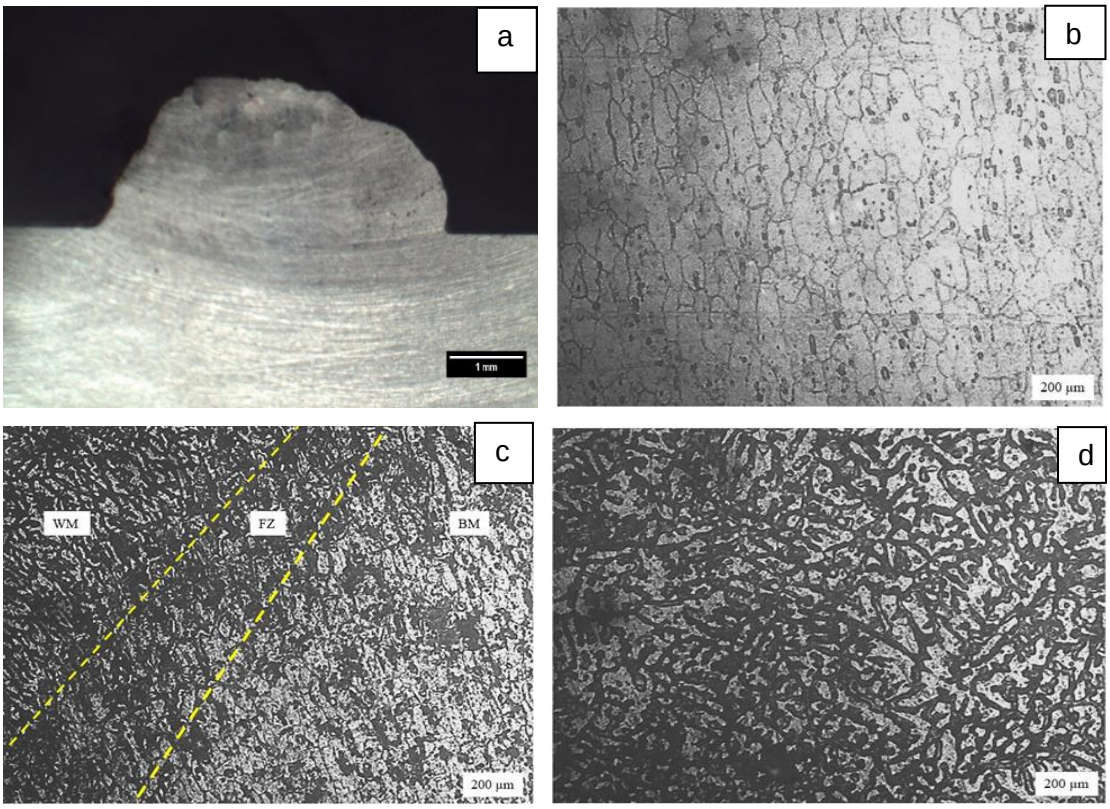

Figure 4.16: (a) FB at 110 A. Microstructure images at 200 µm (b) BM, (c) FZ (d) WZ

4.5. EFFECTS OF PROCESS PARAMETERS

4.5.1. Effect on Heat Input (HI) and Dilution (D)

Heat input (HI) and dilution (D) exhibit a direct relationship, whereby an augmentation in heat input leads to a greater volume of substrate material being melted, consequently resulting in an increase in dilution. Conversely, a decrease in heat input corresponds to reduced dilution. As previously mentioned, dilution is defined as the ratio of the area of penetration to the total area of the weld, as shown in equation (4.1). The dimensions of the weld bead primarily influence this factor. The heat input curve is illustrated in Figure 4.17, while the dilution curve is shown in Figure 4.18 for the weld beads fabricated using both flux and without flux, employing the CMT welding technique with respect to welding speed (S). Heat input is calculated using equation (4.2) to determine the relationship between these factors. The influence of welding speed on various factors such as plate deformation, thickness of heat-affected zone (HAZ), and arc stability make it an important response in the welding process. Increasing welding speed leads to less dilution, which can be attributed to the lower heat input. Figure 4.17 illustrates that, for both cases, dilution (D) decreases as the welding speed (S) increases from 30-50 cm/min,

due to a decrease in heat input on the weld and less melting of the substrate material, resulting in a smaller penetration area as indicated by macro-images. Conversely, decreasing the welding speed (S) increases the heat input on the base material, causing more melting of the base material and resulting in higher DOP, leading to a higher percentage of dilution. Additionally, an increase in current from 90 A to 110 A results in an increase in dilution for both the cases. This is due to the higher heat input generated by the higher current (as illustrated in Figure. 4.17), leading to the melting of the substrate material for deeper penetration and a subsequent increase in the percentage of dilution.

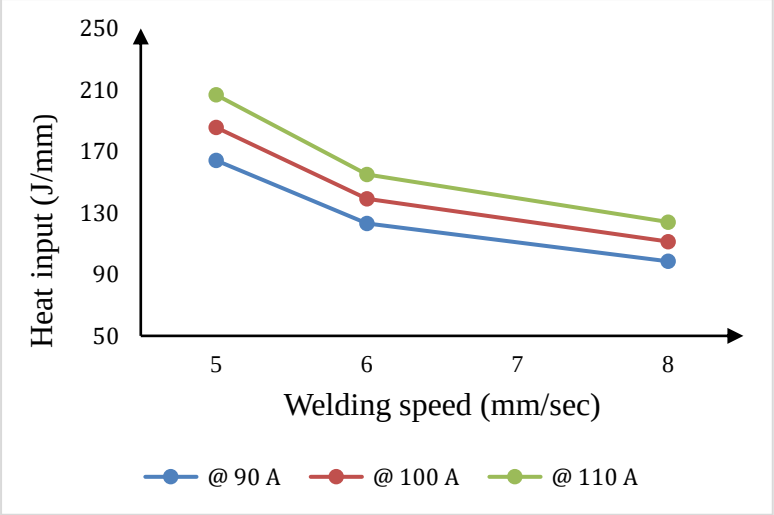

Figure 4.17: Heat input vs welding speed curve

From Figure 4.18, it is evident that as the current is raised from 90 A to 100 A, the dilution of the weld beads formed without flux increases to 9.37% while it increases to 12.03% when weld beads formed using activated flux in comparison to 6.47% for the weld beads formed using without flux while it increases 10.71% when weld beads formed using activated flux w.r.t. weld speed. When comparing current periods of 90-100 A and 100-110 A, higher values of dilution (D) are observed for the former due to a higher heat input, as illustrated in Figure 4.17. The trend of dilution with respect to heat input is clearly demonstrated in Figure 4.19. In this graph, a noticeable change in dilution is observed as the current is increased from 90 A to 100 A across all welding processes. This change in dilution is primarily attributed to the varying heat input.

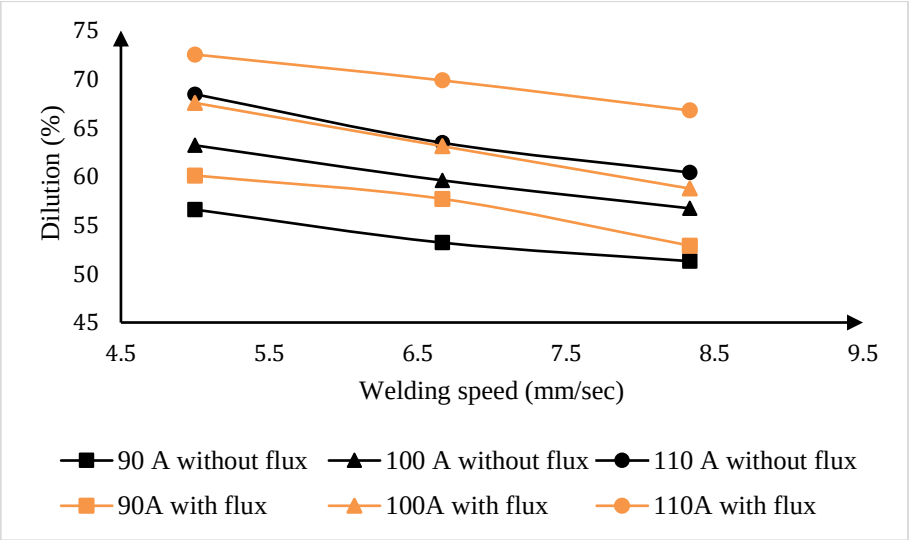

Figure 4.18: Comparison of percentage dilution between weld beads formed without and with flux

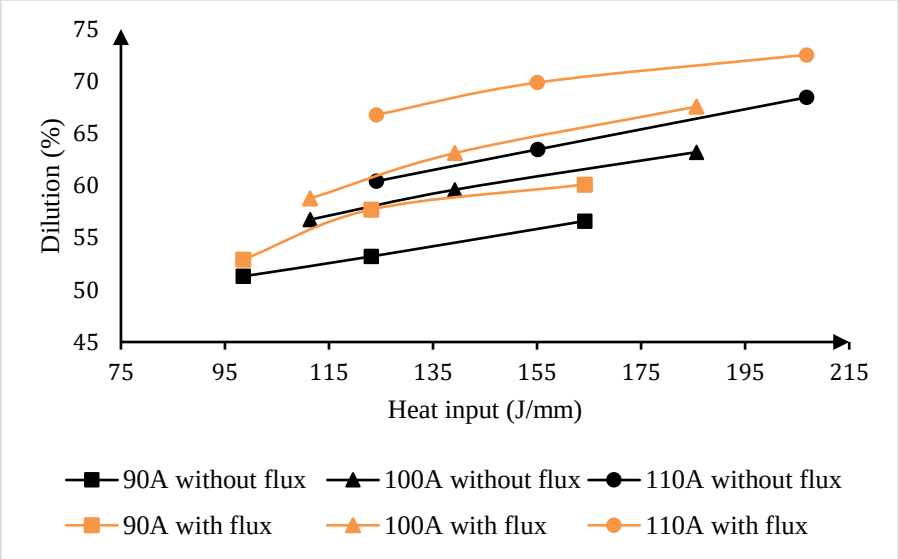

Figure 4.19: Percentage Dilution vs Heat input between weld beads formed without and with flux

4.5.2. Effect on Penetration

Achieving a good joint efficiency depends significantly on penetration, as more depth of penetration results in high efficiency of joint by allowing the filler material to fuse more thoroughly into the substrate material. In order to achieve a superior joint, it is vital to attain deeper penetration and higher tensile strength, while minimizing the heat-affected zone (HAZ), width, and weld reinforcement to reduce the consumption of weld metal. This requirement holds true for all types of welding [40]. As depicted in Figure 4.20, it is commonly observed that penetration is positively affected by a decrease in welding speed, and an increase in welding current.

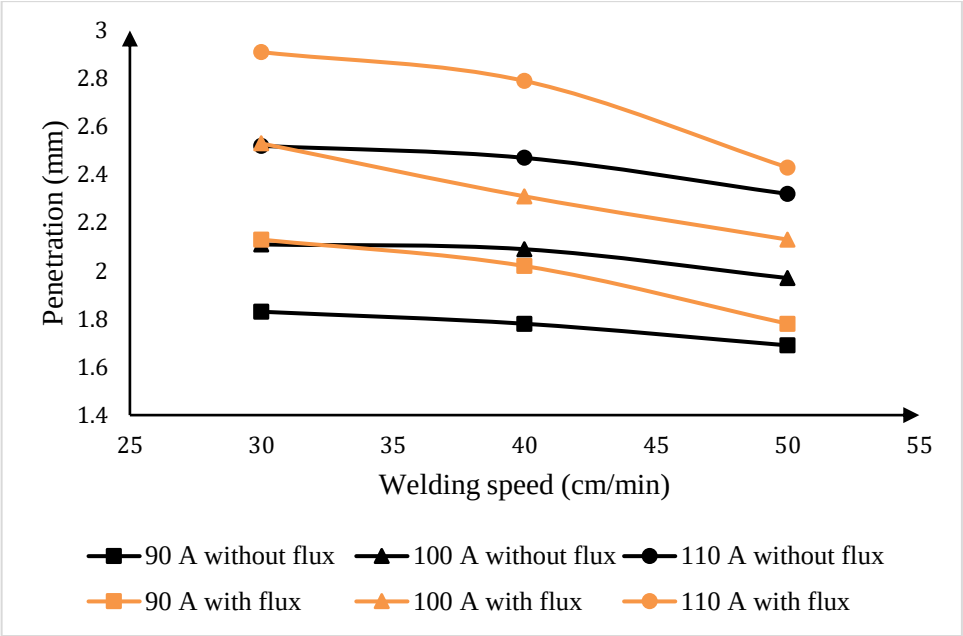

Figure 4.20: Comparison of penetration between weld beads formed without and with flux

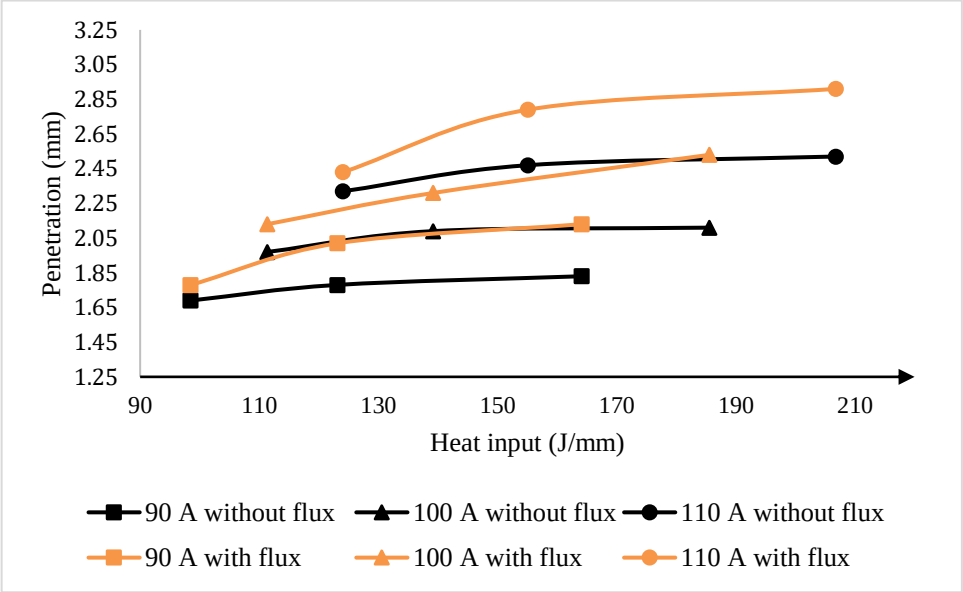

Figure 4.21: Penetration vs Heat input between weld beads formed without and with flux

The Wire Feed Rate (WFR) also has a crucial role in enhancing the penetration. As the WFR increases, the current also increases, causing an elevated heat input during the welding process. This, in turn, results in more substrate material melting. When it comes to CMT welding, the oscillatory movement of the wire plays a crucial role in controlling the penetration by managing the length of arc. In CMT, a higher wire feed rate results in increased current, leading to more frequent droplet detachments and consequently deeper penetration. As depicted in Figure 4.21, it is observed that weld beads formed using activated flux achieve a comparable level of penetration to those formed without flux, but with a lower amount of heat input, thereby resulting in energy savings.

4.5.3. Effect on Micro-hardness

The heat input during the welding of AA6082 base plate with ER4043 filler wire can have an effect on the microhardness of the weld. Heat input refers to the amount of energy transferred to the base metal during the welding process, and it is influenced by factors such as welding current, voltage, welding speed, and travel angle. In general, increasing the heat input in the welding process can lead to changes in the microstructure of the weld, which can subsequently affect the microhardness.

The current and welding speed in CMT (Cold Metal Transfer) welding can both influence the microhardness of a weld. At higher welding currents CMT welding generally result in increased microhardness in the weld zone. This is due to the higher heat input, which leads to more complete fusion and refinement of the microstructure. However, excessively high currents can also cause overheating and potential issues like increased heat-affected zone size and weld defects [60]. Therefore, it is important to find the optimal current range that balances higher microhardness with acceptable weld quality. The welding speed in CMT welding refers to the rate at which the welding torch moves along the joint. Increasing the welding speed typically leads to a decrease in microhardness. This is because a higher welding speed results in less heat input and shorter heat exposure time, which may not allow for sufficient diffusion and grain refinement in the weld zone. Conversely, slower welding speeds provide more time for heat transfer and allow for better microstructural development, resulting in higher microhardness [61]. It is worth noting that the microhardness of a weld is influenced by various other factors such as base metal composition, heat treatment, and post-welding processes. Therefore, optimizing both the current and welding speed in CMT welding requires careful consideration of these factors to achieve the desired microhardness and overall weld quality.

It is observed from Figure 4.22 that as we move from sample 1 to 3 there is an increase in welding speed which leads to decrease in total heat input. This reduced heat input results in lower micro hardness. But for the same process parameters, the weld beads fabricated using flux gives more hardness. The main reason behind this is when we apply SiC layer as activated flux, due to more affinity of ER4043 and AA6082 towards silicon, it easily deposited and mixed properly inside the weld pool. Due to which the pores formation limits to negligible in comparison to those without activated flux. Process parameters corresponding to sample number can be seen from Table 3.4.

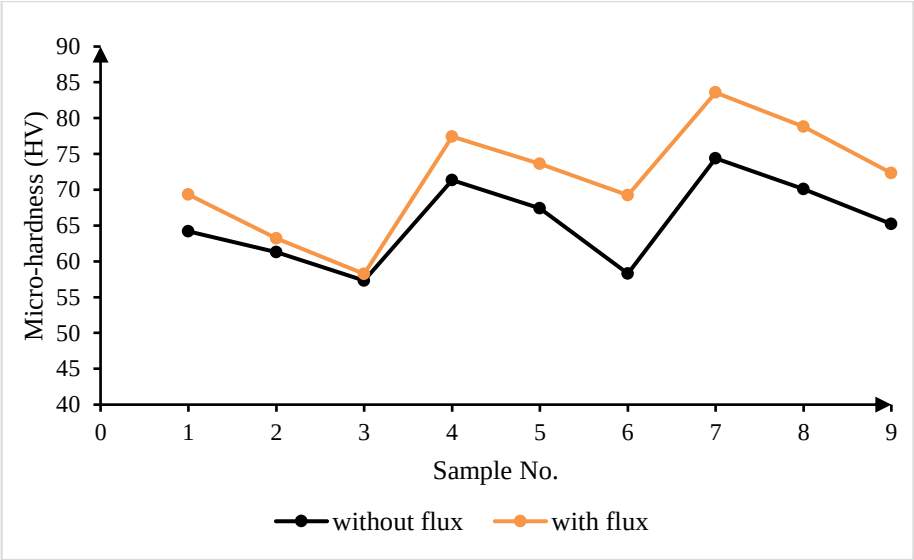

Figure 4.22: Comparison of penetration between weld beads formed without and with flux

Microhardness analysis is also carried out on the optimized process parameter at which welding current is 110 A and the welding speed is 30 cm/min and the gas flow rate is kept constant at 15 ltr/min. Vickers hardness testing with load of 300 gm is employed for testing with indentation time of 10s. Total eight indentations has been made on one specimen from centre of weld bead to base metal, as shown in Figure 4.23, and five indents are also made to check the variation of hardness in vertical direction as own in Figure 4.24.

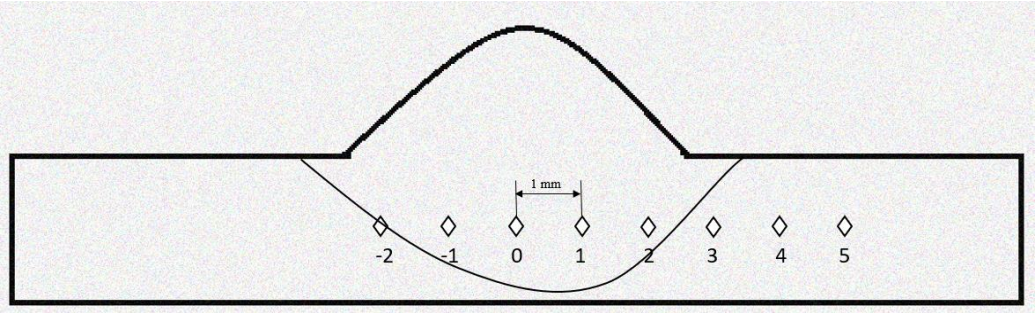

Figure 4.23: Hardness testing at various points taken in horizontal direction

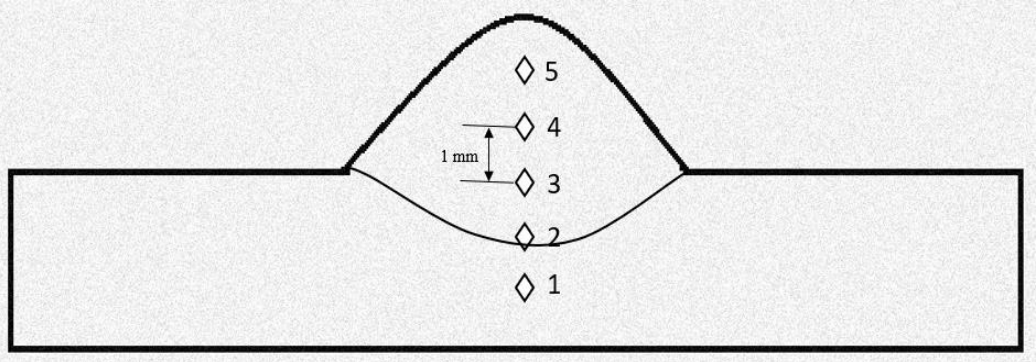

Figure 4.24 Hardness testing at various points taken in vertical direction

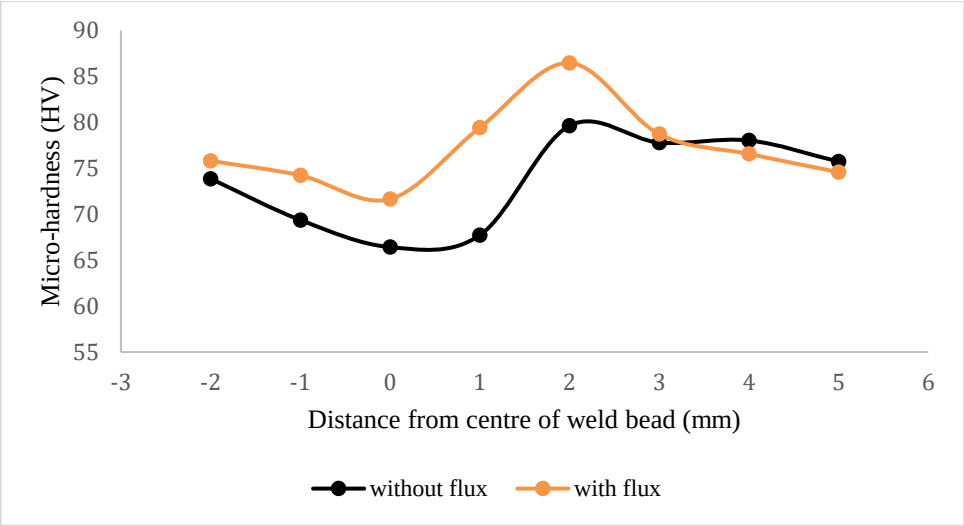

Figure 4.25: Weld bead hardness distribution in horizontal direction

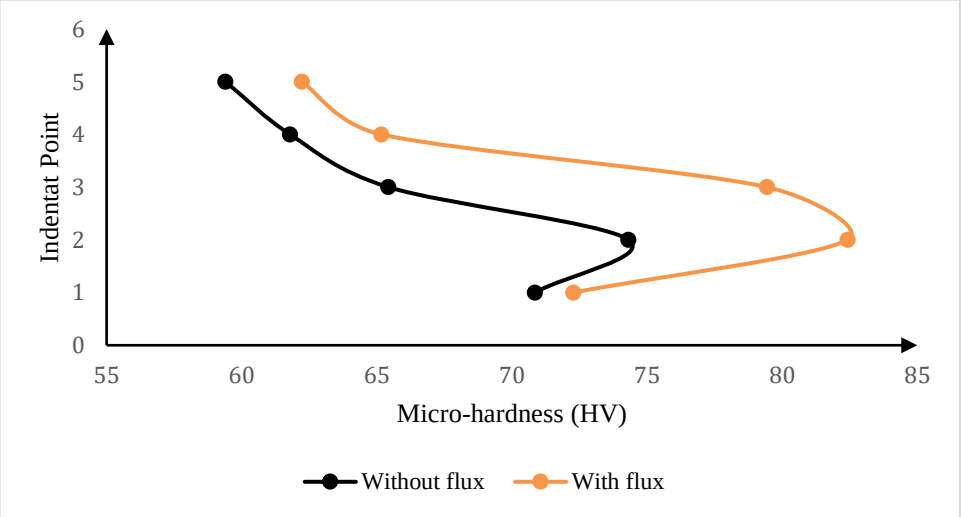

Figure 4.26: Weld bead hardness distribution in vertical direction

From the Figure 4.25, it is clearly seen that how the hardness varying from center of weld bead to BM. This graph is corresponding to Figure 4.23. At the bead center the hardness is very less because of coarse grains. As we move towards FZ, the size of grain decreases which results in higher micro-hardness. There is little variance in micro-hardness of BM when comparing both the cases. Also, from Figure 4.26, it is seen that as we come vertically downwards from weld bead to base metal, the hardness increases up to the fusion zone as the size of grain decreases in fusion zone which results in more hardness.

CHAPTER 5

CONCLUSION AND FUTURE SCOPE

5.1 Conclusion

In this research, metal matrix composite samples were produced using an active flux and the wire cold metal transfer (CMT) process. The focus of the study was to examine the impact of SiC particles on grain orientation, grain evolution, and mechanical properties. A comparison was made with samples that were deposited in their original state. The following findings were deduced:

1. Weld beads fabricated using activated flux has higher penetration and reduced bead width in comparison to those which obtained using without flux for the same current and welding speed. To enhance joint efficiency, it is essential to achieve sufficient dilution and penetration while minimizing the heat input.
2. The macrostructure, microstructure, and hardness of the bead on plate welds were significantly influenced by the use of activated flux.
3. Taguchi method is used to optimize process parameter that affects the dilution and microhardness of AA6082 alloy joint with filler wire ER4043.
4. The optimal process parameters are 110 A and 30 cm/min for dilution and 90 A and 50 cm/min for micro-hardness.
5. With the optimal process parameters, the dilution is 66.74% and micro-hardness is 71.86HV for weld bead formed without using flux. But the dilution is 75.2% and microhardness is 79.77 HV for the weld bead formed using flux.
6. The relationship between current and penetration is directly proportional, while the relationship between welding speed and penetration is inversely proportional. When considering weld speed, the percentage increase in penetration is significantly higher compared to the welding current. Overall, use of active flux in weld beads results in reduced weld width and higher penetration for the same current and welding speed compared to those which formed without using active flux.

5.2 Scope for Future Work

1. The setup can be adjusted to accommodate different process parameters, including the utilization of various filler wire types, fine-tuning the contact tip to workpiece distance (CTWD), etc. These modifications can lead to improved mechanical properties and desired outcomes.
2. Aluminum composites can be manufactured by incorporating natural or synthetic reinforcements, followed by the implementation of welding processes.
3. Further exploration is required to examine the impact of preheating and post-heating on achieving optimal joint quality when welding aluminium alloys.
4. The application of robotic CMT enables the precise and accurate joining of metals.
5. To attain more precise outcomes, the optimization process can be conducted using artificial neural network (ANN) in conjunction with genetic algorithm (GA).

REFERENCES

[1]. Elrefaey A, and Ross NG; Microstructure and mechanical properties of cold metal transfer welding similar and dissimilar aluminium alloys; *Acta Metall. Sin-Engl*. 2015 28 715-724.

[2]. Mcauley JW; Global sustainability and key needs in future automotive design; *Environ. Sci. Technol*. 2003 37 5414- 5416.

[3]. Selvamani ST, Govindarajan P, Ajaymohan M, Hariharan SJ, and Vigneshwar M; Correlation between Micro hardness and Microstructure of CMT Welded AA 7075 Al Alloy; 2018 In IOP Conference Series: *Materials Science and Engineering* 390 012058.

[4]. Totten GE, and MacKenzie DS; Handbook of aluminium: vol. 1: *Physical metallurgy and processes*; CRC press 2003, New York.

[5]. Kaufman JG; Introduction to aluminium alloys and tempers ASM international 2000, USA.

[6]. Mathers G; The welding of aluminium and its alloys Woodhead publishing 2002, England.

[7]. Summers, P.T., Chen, Y., and Rippe, C.M., "Overview of aluminum alloy mechanical properties during and after fires", Fire Sci Rev, 2015, Vol. 4, No. 3

[8]. Connor LP; Welding Handbook: Vol. 1: Welding Technology; Welding Science and Technology, 9th edition, American Welding Society.

[9]. "Aluminium Welding" by the American Welding Society (AWS). Available at: https://pubs.aws.org/p/1271/aluminum-welding

[10]. https://www.aerospacewelding.com/lynns-blog/tig-vs-mig

[11]. https://www.thermalpowertech.com/2019/10/welding-and-welding-types.html

[12]. Taheri H, Kilpatrick M, Norvalls M, Harper WJ, Koester LW, Bigelow T, Bond LJ. Investigation of Nondestructive Testing Methods for Friction Stir Welding. *Metals*. 2019; 9(6):624.

[13]. Liu, K.; Jiang, X.; Chen, S.; Effect of SiC addition on microstructure and properties of Al-Mg alloy fabricated by powder and wire cold metal transfer process, Journal of Materials research & Technology (2022); 17:310-319

[14]. Lai, H.; Lu, S.; Effect of Brazing Flux Pb on Microstructure and Mechanical Property of CMT Weld-brazed Lap Joint of 5052 Aluminum Alloy to Galvanized Q235 Steel, Materials Science Forum Vol789 (2014) PP 290-296.

[15]. Ruan, Y.; Qiu, X.; Gong, W.; Sun, D.; Mechanical properties and microstructure of 6082-T6 joint welded by twin wire metal inert gas welding with the SiO2 flux, Materials and Design 35 (2012) 20-24.

[16]. Huang, Y.; Yuan, Y.; Feng, Y.; Liu, J.; Cui, L.; Effect of activating flux Cr2O3 on microstructure and properties of laser welded 5083 aluminum alloys; Optics & laser technology 150 (2022) 107930.

[17]. Madavi, K.R.; Jogi, B.; Lohar, G.; Investigational study and microstructural comparison of MIG welding process for with and without activated flux; Materials Today Proceedings 51 (2022) 212-216.

[18]. Chakraborty, A.; Sharma, C.; Srivastava, M.; Influence of activated flux on weld bead hardness of MIG welded austenitic stainless steel, Materials Today Proceedings 47 (2021) 6884-6888.

[19]. Baghel, A.; Sharma, C.; Rathee, S.; Influence of activated flux on micro-structural and mechanical properties of AISI 1018 during MIG welding, Materials Today Proceedings 47 (2021) 6947-6952.

[20]. Huang, H.; Effects of activating flux on the welded joint characteristics in gas metal arc welding, Materials and Design 31 (2010) 2488-2495.

[21]. Vasudevan, M.; Dwivedi, D.; Vidyarthy, R.; Influence of M-TIG and A-TIG Welding Process on Microstructure and Mechanical Behavior of 409 Ferritic Stainless Steel; Journal of Materials Engineering and Performance Vol 26(3) March 2017 1391-1403.

[22]. Rathee, S.; Srivastava, M.; Sharma, C.; Activated flux TIG welding of dissimilar SS202 and SS304 alloys: Effect of oxide and chloride fluxes on microstructure and mechanical properties of joints, Materials Today: Proceedings 47 (2021) 7189-7195.

[23]. Huang, H.; Effects of shielding gas composition and activating flux on GTAW weldments; Materials and Design 30 (2010) 2404-2409.

[24]. Kulkarni, A.; Dwivedi, D.; Vidyarthy, R.S.; Study of microstructure and mechanical property relationships of A-TIG welded P91–316L dissimilar steel joint; Materials Science and Engineering A 695 (2017) 249-257.

[25]. Vinothkumar, H.; Balakrishnan, M.; Gulanthaivel, K.; Mohanraj, R.; Investigation on effects of flux assisted GTAW welding process on mechanical, metallurgical characteristics of dissimilar metals SS 304 and SS 316 L; Materials Today: Proceedings 33 (2020) 3191-3196.

[26]. Vidyarthy, R.S.; Sivateja, P.; Influence of activating flux tungsten inert gas welding on mechanical and metallurgical properties of the mild steel; Materials Today: Proceedings 28 (2020) 977-981.

[27]. Vasudevan, M.; Effect of A-TIG Welding Process on the Weld Attributes of Type 304LN and 316LN Stainless Steels; Journal of Materials Engineering and Performance (2017) 1325-1336.

[28]. Grubisa, L.; Bajic, D.; Vuherer, T.; Influence of activating flux on the mechanical properties of the plasma welded joint of Austenitic steel; Procedia Structural Integrity 13 (2018) 430-437.

[29]. Zhang, Z.; Cao, Q.; Study on metal transfer behaviour in metal inert gas arc welding with activating flux for magnesium alloy, Science and Technology of Welding and Joining (2012).

[30]. Ramkumar, K.; Kumar, B.; Dev, S,; Studies on the weldability, microstructure and mechanical properties of activated flux TIG weldments of Inconel 718; Materials Science & Engineering A 639 (2015) 234-244.

[31]. Pate, D.; Jani, S.; Shah, D.; Augmentation in depth of penetration of Hastelloy C-22 by FATIG welding; Advances in Industrial and Manufacturing Engineering 4 (2022) 100081.

[32]. Chattopadhyay, A.; Sarkar, S.; Nath, A.; Effect of active flux MgF2 on weld geometry and joint strength in laser beam welding of titanium; Materials Today: Proceedings 41 (2021) 301-306.

[33]. Rakesh, N.; Mohan, A.; Nambiar, S,; Rameshkumar, K.; Effect of fluxes on weld penetration during TIG welding – A review; Materials Today: Proceedings 72 (2023) 3040-3048.

[34]. Patel, N.; Vora, J.; Badheka, V.; Upadhyay, G.; Review on the use of activated flux in arc and beam welding processes; Materials Today: Proceedings 43 (2021) 916-920.

[35]. Westermann, I.; Hopperstad, O.; Langseth, M.; (2014). Mechanical behaviour of an AA6082 aluminium alloy at low temperatures; *Materials Science Forum* 794-796:532-537.

[36]. Pickin, C. G., Williams, S. W., & Lunt, M. (2011). Characterisation of the cold metal transfer (CMT) process and its application for low dilution cladding. *Journal of Materials Processing Technology*, 211(3), 496-502.

[37]. Cao, R., Wen, B. F., Chen, J. H., & Wang, P. C. (2013). Cold metal transfer joining of magnesium AZ31B-to-aluminum A6061-T6. *Materials Science and Engineering: A*, 560, 256-266.

[38]. https://support.minitab.com/en-us/minitab/20/help-and-how-to/statistical-modeling/doe/supporting-topics/taguchi-designs/taguchi-designs/

[39]. Pickin, C. G., Williams, S. W., & Lunt, M. (2011). Characterisation of the cold metal transfer (CMT) process and its application for low dilution cladding. *Journal of Materials Processing Technology*, 211(3), 496-502.

[40]. Wang, J., Feng, J. C., & Wang, Y. X. (2008). Microstructure of Al–Mg dissimilar weld made by cold metal transfer MIG welding. Materials Science and Technology, 24(7), 827-831.

[41]. https://www.wermac.org/materials/vickers.html

[42]. Greyjevo, O. G. T. V. Z., & Metodo, A. I. T. (2009). Optimization of weld bead 202 geometry in TIG welding process using grey relation analysis and Taguchi method. *Materiali in tehnologije*, 43(3), 143-149.

[43]. Hunt, A. C., Kluken, A. O., & Edwards, G. R. (1994). Heat input and dilution effects in microalloyed steel weld metals. *WELDING JOURNAL-NEW YORK-*, 73, 9- s

[44]. Saha, M. K., Hazra, R., Mondal, A., & Das, S. (2019). Effect of heat input on geometry of austenitic stainless steel weld bead on low carbon steel. *Journal of The Institution of Engineers (India): Series C*, 100(4), 607-615.

[45]. Sun, Q. J., Li, J. Z., Liu, Y. B., Li, B. P., Xu, P. W., & Feng, J. C. (2017). Microstructural characterization and mechanical properties of Al/Ti joint welded by CMT method—Assisted hybrid magnetic field. *Materials & Design*, 116, 316-324.

[46]. Cook, G. E., & Eassa, H. E. D. E. (1985). The effect of high-frequency pulsing of a welding arc. *IEEE Transactions on Industry Applications*, (5), 1294-1299.

[47]. İrizalp, A. O., Durmuş, H., Yüksel, N., & Türkmen, İ. (2016). Cold metal transfer welding of AA1050 aluminum thin sheets. *Matéria (Rio de Janeiro)*, 21(3), 615-622.

[48]. Mendez, P. F., & Eagar, T. W. (2001). Welding processes for aeronautics. *Advanced materials and processes*, 159(5), 39-43.

[49]. Quintino, L., Liskevich, O., Vilarinho, L., & Scotti, A. (2013). Heat input in full penetration welds in gas metal arc welding (GMAW). The International *Journal of Advanced Manufacturing Technology*, 68(9), 2833-2840

[50]. Joseph, A., Harwig, D., Farson, D. F., & Richardson, R. (2003). Measurement and calculation of arc power and heat transfer efficiency in pulsed gas metal arc welding. *Science and Technology of Welding and Joining*, 8(6), 400-406.

[51]. Adak, D. K., Mukherjee, M., & Pal, T. K. (2015). Development of a direct correlation of bead geometry, grain size and HAZ width with the GMAW process parameters on bead-on-plate welds of mild steel. *Transactions of the Indian Institute of Metals*, 68(5), 839-849.

[52]. Utkarsh, S., Neel, P., Mahajan, M. T., Jignesh, P., & Prajapati, R. B. (2014). Experimental investigation of MIG welding for ST-37 using design of 211 experiment. *International Journal of Scientific and Research Publications*, 4(5), 1-4.

[53]. Gunaraj, V., & Murugan, N. (1999). Prediction and comparison of the area of the heat-affected zone for the bead-on-plate and bead-on-joint in submerged arc welding of pipes. *Journal of Materials Processing Technology*, 95(1-3), 246-261.

[54]. Goyal, H., Mandal, N., Roy, H., Mitra, S. K., & Mondal, B. (2015). Multi response optimization for processing Al–SiCp composites: an approach towards enhancement of mechanical properties. *Transactions of the Indian Institute of Metals*, 68(3), 453- 463.

[55]. Anyalebechi, P. N. (1995). Analysis of the effects of alloying elements on hydrogen solubility in liquid aluminum alloys. *Scripta metallurgica et materialia*, 33(8), 1209- 1216.

[56]. B. Cong, J. Ding and S. Williams, Effect of Arc Mode in Cold Metal Transfer Process on Porosity of Additively Manufactured Al-6 3 % Cu Alloy, *Int. J. Adv. Manuf. Technol.*, 2015 https://doi.org/10.1007/ s00170-014-6346-x

[57]. M. Vasudevan, Effect of A-TIG welding process on the weld attributes of type 304LN and 316LN stainless steels, *J. Mater. Eng. Perform*. 26 (2017) 1325–1336

[58]. Ahmad, R., & Bakar, M. A. (2011). Effect of a post-weld heat treatment on the mechanical and microstructure properties of AA6061 joints welded by the gas metal arc welding cold metal transfer method. *Materials & Design*, 32(10), 5120-5126.

[59]. Maisonnette, D., Suery, M., Nelias, D., Chaudet, P., & Epicier, T. (2011). Effects of heat treatments on the microstructure and mechanical properties of a 6061-aluminium alloy. *Materials Science and Engineering*: A, 528(6), 2718-2724.

[60]. Kokabi, A.; Saeid, T.; Effect of welding speed on microstructure and mechanical properties of friction stir welded 7075 aluminum alloy; *Materials Science and Engineering* 2014.

[61]. Yong He, Xianming Zhang, Xuan Wang, Jun Liu, Wenxian Li; Effect of heat input on microstructure and mechanical properties of AA6082-T6 aluminum alloy welded by pulsed GTAW; *Materials and Design*; 2013.

[62]. Mossman MM and Lippold JC; Weldability testing of dissimilar combinations of 5000-and 6000-series aluminium alloys; *Weld. J. New York* 2002 81 188-194.

[63]. D. Adak, Mukherjee, M., & Pal, T. K. (2015). Development of a direct correlation of bead geometry, grain size and HAZ width with the GMAW process parameters on bead-on-plate welds of mild steel. *Transactions of the Indian Institute of Metals*, 68(5), 839-849.

[64]. Ahmad, R., & Bakar, M. A. (2011). Effect of a post-weld heat treatment on the mechanical and microstructure properties of AA6061 joints welded by the gas metal arc welding cold metal transfer method. *Materials & Design*, 32(10), 5120-5126.

[65]. Ahsan, M. R., Kim, Y. R., Kim, C. H., Kim, J. W., Ashiri, R., & Park, Y. D. (2016). Porosity formation mechanisms in cold metal transfer (CMT) gas metal

arc welding (GMAW) of zinc coated steels. *Science and Technology of Welding and Joining*, 21(3), 209-215.

[66]. Kumar NP, Chinnadurai T, Vendan SA, and Shanmugam NS; Techno Economical Evaluation for Energy Analysis in AA6061 during Cold Metal Transfer Welding; *Materials Today: Proceedings* 2018 5(11) 23375-23383.

[67]. Allison, A., & Scudamore, R. (2014). Strategic Research Agenda: Joining: Joining Sub-platform. Available from (http://www.joining-platform.com/documents/ Joining%20Sub-Platform%20SRA%20-%202014.pdf).

[68]. K.D. Ramkumar, P.S. Goutham, V.S. Radhakrishna, A. Tiwari, S. Anirudh, Studies on the structure–property relationships and corrosion behaviour of the activated flux TIG welding of UNS S32750, *J. Manuf. Process*. 23 (2016) 231– 241

[69]. Ding, J.; Colegrove, P.; Mehnen, J.; Ganguly, S.; Almeida, P.S.; Wang, F.; Williams, S. Thermo-mechanical analysis of Wire and Arc Additive Layer Manufacturing process on large multi-layer parts. *Comput. Mater. Sci*. 2011, 50, 3315–3322

[70]. Ríos, S.; Colegrove, P.A.; Williams, S.W. Metal transfer modes in plasma Wire + Arc additive manufacture. *J. Mater. Process. Technol*. 2019, 264, 45–54.

[71]. A.C.M. Bekker and J.C. Verlinden, Life Cycle Assessment of Wire + arc Additive Manufacturing Compared to Green Sand Casting and CNC Milling in Stainless Steel, *J. Clean. Prod.*, 2018, 177, p 438– 447.